Chaos
An Interdisciplinary Journal
of Nonlinear Science

RESEARCH ARTICLE | NOVEMBER 09 2021

Soliton-like structures in the spectrum and the corresponding eigenstates morphology for the quantum desymmetrized Sinai billiard

M. R. Sales ; A. L. Azevedo ; F. Teston; M. G. E. da Luz ; F. M. Zanetti

Chaos 31, 113122 (2021)
https://doi.org/10.1063/5.0063628

Chaos ARTICLE scitation.org/journal/cha

Soliton-like structures in the spectrum and the corresponding eigenstates morphology for the quantum desymmetrized Sinai billiard

Cite as: Chaos **31**, 113122 (2021); doi: 10.1063/5.0063628
Submitted: 15 July 2021 · Accepted: 19 October 2021 ·
Published Online: 9 November 2021

View Online Export Citation CrossMark

M. R. Sales,[a] A. L. Azevedo, F. Teston, M. G. E. da Luz,[b] and F. M. Zanetti

AFFILIATIONS

Departamento de Física, Universidade Federal do Paraná, Curitiba, PR 81531-980, Brazil

[a]**Present address:** Departamento de Física, Universidade Estadual de Ponta Grossa, Ponta Grossa, PR 84030-900, Brazil.
[b]**Author to whom correspondence should be addressed:** luz@fisica.ufpr.br

ABSTRACT

By continuously varying certain geometric parameters γ of the totally desymmetrized quantum Sinai billiard, we study the formation of the so-called soliton-like structures in the spectra of the resulting family of systems. We present a detailed characterization of the eigenstate ψ_n morphologies along such structures. Usually, scarring and bouncing ball mode states are expected to fully explain the solitons. However, we show that they do not exhaust all the possibilities. States with strong resemblance to very particular solutions of the associated integrable case (45°–45° right triangle) also account for the ψ_n's. We argue that for the emergence of the solitons, in fact, there must be an interplay between the spatial localization properties of the soliton-related ψ_n's and the rescaling properties of the billiards with γ. This is illustrated, e.g., by comparing the behavior of the eigenwavelengths along the solitons and the billiard size dependence on γ. Considerations on how these findings could extend to other type of billiards are also briefly addressed.

An important class of problems for the general understanding of deterministic chaos is formed by the so called billiard tables: a particle confined in a free region delimited by a closed hard boundary. In the broad context of quantum chaology, by solving the Schrödinger equation and then analyzing statistical properties of the eigenenergies $\{E_n\}$ and special features of the eigenstates ψ_n's, one can establish the system's regular or chaotic character. Although less explored, it is also possible to investigate a whole family of models by changing a certain associated parameter γ (e.g., an angle or a side length of a billiard border). Then, one might infer chaotic properties from correlations between groups of E_n's and specific patterns for subsets of ψ_n's as a function of γ. We conduct this latter type of study for the paradigmatic chaotic Sinai billiard in its fully desymmetrized version: a right triangle with one acute angle substituted by a concave arc of circle. As γ varies, we find structures for the billiards known in the literature as spectra solitons. Through comprehensive analysis, we show how these solitons are associated with the morphologies, "shapes," of special eigenstates of the related (and not chaotic) right triangles. We explain such emergence based on simple geometric arguments and the localization behavior of the involved ψ_n's. The mechanisms generating the present phenomenology conceivably could also result in similar effects in other chaotic systems.

I. INTRODUCTION

Deterministic chaos[1] (hereafter just chaos), both in classical and quantum physics,[2] is a rather fundamental area in the broad realm of dynamical systems,[3,4] e.g., essentially encompassing the whole of chaotic Hamiltonian evolution.[5,6] The number of distinct problems displaying chaos is overwhelming.[7] Particularly, billiard systems[8–13] are of paramount importance to unveil fundamental aspects of chaotic behavior. In its simplest 2D formulation, one considers a point-like particle of mass μ confined in a planar finite region Ω for which the potential $V(\mathbf{r} \in \Omega) = 0$. The region Ω is delimited by hard wall borders $\partial\Omega$. Classically, given the energy E, we shall determine the global properties of the particle possible Newtonian trajectories in the phase space, supposing specular reflections from $\partial\Omega$. Quantically, we shall obtain the eigenfunctions and eigenvalues of the Helmholtz equation $(\nabla^2 + k^2)\psi(\mathbf{r}, k) = 0$

in Ω (for $k^2 = 2\mu E/\hbar^2$), assuming Dirichlet boundary conditions, namely, $\psi(\mathbf{r} \in \partial\Omega) = 0$.

Because of the relative structural simplicity of billiards—if compared to more involving systems[14] or (e.g., in the quantum case) if within Ω, either there is more than one particle[15] or deformation or elastic potentials are present[16–18]—the emergence or not of chaotic behavior is fully dictated by the geometric features of $\partial\Omega$.[10,13] For instance, in the classical context, elements of hard chaos (e.g., ergodicity, positive Kolmogorov–Sinai entropy, mixing, etc.[19]) arise from boundaries $\partial\Omega$, which are everywhere dispersing.[20] Also, the unfolding of chaos due to defocusing effects is a direct consequence of certain particularities of $\partial\Omega$.[21] In fact, dispersing and defocusing have been proposed to exhaust all the mechanisms creating chaotic dynamics in classical billiards.[22]

On the other hand, in quantum chaology[23] or quantum wave chaos,[24] the signatures[25] of "quantum chaos" are associated with the spectrum $\{E_n\}$ statistical features and morphological aspects of the eigenstates ψ_n.[2,5,24,26] However, the situation is not different regarding the fundamental importance of the billiard shapes: $\partial\Omega$ fully establishes the specificities of the Helmholtz operator eigensolutions.[24,27] Therefore, the peculiarities of such eigensolutions[28] are expected to be qualitatively distinct if the corresponding classical billiards are or are not chaotic.[29]

The above broad (thus, not limited to billiard models) interplay between classical and quantum chaos is manifested in distinct measures associated with the spectrum statistical properties of the latter. We just mention the distribution of nearest-neighbor "unfolded"[2,30] distances s between successive levels, $P(s)$. For the quantum counterpart of classically regular systems, the Berry–Tabor considerations[31] predict the Poisson distribution $P(s) = \exp[-s]$, which for some examples can be put in very rigorous grounds.[32] Conversely, for the chaotic case, the Bohigas–Giannoni–Schmit conjecture[33] points to universal features for the spectrum correlations, provided generic symmetries are preserved; exactly those considered in random matrix theory (RMT).[34] In particular, for problems with time-reversal invariance $P(s) = (\pi/2)\, s \exp[-\pi s^2/4]$, which is the Wigner–Dyson expression for the RMT Gaussian orthogonal ensemble (GOE) (see also Sec. IV). Such conjecture has a sound semiclassical justification.[35]

Individual ψ_n's can also display distinguished morphologies for chaotic problems.[2,6,24,26,36] A remarkable proposal by Berry[37] is that high energy eigenfunctions of chaotic systems may exhibit certain aspects similar to those of a linear combination of random plane waves. By the same token, the distribution of wave function nodal domain[38–40] should discriminate between regular and chaotic quantum dynamics. We also mention Heller's scarred eigenstates,[41] namely, certain ψ_n's concentrated on the loci of the underlying classical system unstable periodic orbits.[42] This has been detected in many distinct billiards[43–47] as well as in other problems.[28,48–50]

The above summarizes the identification of quantum chaos in terms of either global statistical trends of the spectrum or characteristic attributes of the eigenstates. Less common, however, are investigations trying to link certain sets of eigenvalues with special features of groups of eigenstates (notwithstanding, for interesting works in this direction, see, e.g., Refs. 51–55). Yet, this should not be a surprise: for an arbitrary chaotic system, one could not expect recurrent appearance[56,57] of general relations between subsets of $\{E_n\}$ and specific spatial pattern properties carrying over collections of ψ_n's.[58–60]

The situation may be different if instead of just one, we address a full family of systems. In fact, suppose a quantum problem depending on a parameter γ. In this case, the dynamics of the "trajectories" $E_n(\gamma)$'s [or $k_n(\gamma)$] as a function of γ can display a rich phenomenology—e.g., resembling the many-body classical evolution of repulsively interacting particles confined to a box—especially when distinct γ's lead to chaotic behavior.[61–64] Such a picture of $k_n \times \gamma$ as paths in the parameter space was originally devised[61,62] for Hamiltonians in the form $H = H_0 + \gamma V$. Nonetheless, it works also well for γ simply being a geometric parameter of a billiard.[65,66] Under the above framework, distinct properties can be addressed. An example is the distribution of curvatures $\mathscr{P}(|K|)$,[67] with K representing the degree of sinuosity of the trajectories $\{k_n(\gamma)\}$. For irregular spectra, one finds an ubiquitous power-law $\mathscr{P}(|K|) \sim |K|^{-\mu}$ for large $|K|$. The precise constant value of the exponent μ depends on the system general class of symmetry [one of the three, orthogonal ($\mu = 3$), unitary ($\mu = 4$), and symplectic ($\mu = 6$), of the RMT].[65,67] The trajectories with lower $|K|$'s (i.e., more rectilinear-like paths) tend to yield a non-universal behavior for $\mathscr{P}(|K|)$.

Actually, the trajectories of smaller curvature are often associated with the appearance of soliton-like structures in $\{k_n(\gamma)\}$,[65,68] which by their turn are related to certain characteristics of the corresponding eigenfunctions[69,70] (in particular for those in the vicinity of the levels avoided crossing,[71] details in Sec. III). It has been reported that typical ψ_n's accounting for the solitons are the already mentioned scar states as well as the well known bouncing ball modes.[72–75] Moreover, the non-universality of $\mathscr{P}(|K|)$ for $|K|$ small might be due to the various levels of scarring[69] taking place in quantum chaotic systems.[66,70] For billiards, spectra solitons have been observed, e.g., for the Bunimovich stadium,[65,70] pseudointegrable right-angle polygonal shapes, and the quarter-Sinai.[66]

From the previous considerations, it becomes clear that the full assortment of solitons in the $k_n \times \gamma$ space should not display statistical hallmarks common to broad families of systems. Still, we may speculate whether or not (i) the undulatory-geometric mechanisms originating these structures, (ii) the reason for their connection with special eigenstates, (iii) the necessary features of such eigenstates (e.g., can they be only scars and bouncing ball modes?), and (iv) the conditions determining the soliton proliferation; do constitute fairly general processes, at least in quantum billiards.

To shed some light on these issues, we discuss the Sinai billiard in its totally desymmetrized version (Fig. 1). For a fixed area A, the system geometry allows one to control two distinct geometric parameters γ, the (arc of circle) radius r, and the (opposite corner) angle α. By investigating representative energy intervals and ranges for α and r, we identify various soliton-like structures. We perform a detailed characterization of the associated set of eigenstates $\{\psi_n\}$ as, for instance, their spatial pattern changes in the neighborhood of avoided crossings. Besides scars, we also have as such ψ_n's "memory" states, i.e., ψ_n's maintaining the shape of particular solutions of the integrable case ($r = 0$ and $\alpha = 45^\circ$). We discuss aspects related to (i)–(iv) above, focusing on which features should account for the formation of the soliton-like structures. We finally

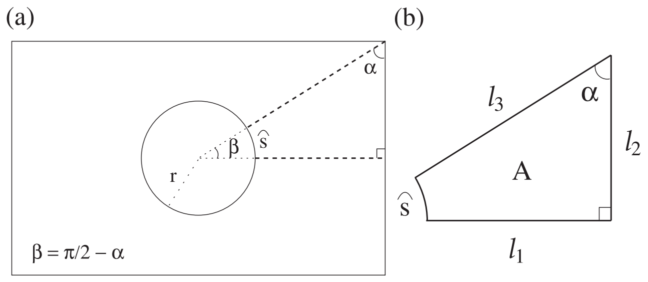

FIG. 1. (a) The usual Sinai billiard, whose domain Ω corresponds to the region inside the rectangle but outside the disk (of radius r). (b) Its complete desymmetrized version, having area A and sides l_1, l_2, l_3, and $\widehat{s}$, this latter actually an arc of circle.

briefly comment on how these findings would potentially extend to other billiards. Once the necessary numerical accuracy is assured, the specific protocol used for the computations is not really essential. Nonetheless, for all the calculations, we employ the boundary wall method (BWM)[76,77] since it is particularly suitable for this type of study,[78] namely, to obtain billiards eigenvalues when geometric parameters are varied.

This paper is organized as follows: In Sec. II, we present the system. A comprehensive set of results is given in Sec. III. Based on these results, in Sec. IV, we address the phenomenology underlying the emergence of the soliton-like structures. Finally, a few remarks and conclusion are drawn in Sec. V.

II. THE QUANTUM DESYMMETRIZED SINAI BILLIARD

We consider the paradigmatic Sinai billiard[20] whose quantum case has been first investigated in Ref. 79. Assume a disk of radius r centered within a rectangle of sides greater than $2r$ [Fig. 1(a)]. For the usual Sinai billiard, Ω corresponds to the intersection between the disk exterior and the rectangle interior regions. Our goal is to discuss the behavior of the wavenumber spectrum $\{k_n\}$ (for $k_n^2 = E_n$ since we set $2\mu/\hbar^2 = 1$) as well as of the associated eigenfunctions $\{\psi_n\}$ resulting solely from specific changes in the system geometric parameters γ. We shall avoid eventual eigenvalue degeneracies due to distinct symmetry families for the ψ_n's, e.g., the wavefunctions being even or odd about the parallel and perpendicular axes passing through the billiard center. Therefore, we restrict our analysis to the desymmetrized Sinai billiard depicted in Fig. 1(b). Essentially, it corresponds to a right triangle billiard with one vertex substituted by a concave arc of circle ($\widehat{s}$ in Fig. 1) of angular aperture $\beta = \pi/2 - \alpha$ and radius r. Our parameters γ will then be α and r.

To characterize the $k_n(\gamma)$'s for distinct n's, we should maintain the billiard density of states $\rho(k)$ as invariant as possible while varying γ. This allows, for each quantum level n, one to interpret $k_n(\gamma)$ as a continuous "path" in the parameter space. From the Weyl formula—see, for instance, Ref. 80—the first (second) most important term determining ρ is the billiard area A (perimeter P). Therefore, we fix A and write the billiard sides as (see Fig. 1)

$$l_1 = \sqrt{(2A + (\pi/2-\alpha)r^2)\,\tan[\alpha]} - r,$$
$$l_2 = \sqrt{\frac{2A + (\pi/2-\alpha)r^2}{\tan[\alpha]}}, \tag{1}$$
$$l_3 = \sqrt{\frac{2A + (\pi/2-\alpha)r^2}{\cos[\alpha]\,\sin[\alpha]}} - r.$$

Note that $(l_1+r)^2 + l_2^2 = (l_3+r)^2$ and that the quantity $((l_1+r)\times l_2)/2 - (\pi/2-\alpha)/2 \times r^2$—the expression for the billiard area—properly gives A. The perimeter reads $P = l_1 + l_2 + l_3 + (\pi/2-\alpha)\,r$. For the aspects we are going to analyze, in the calculations, it is enough to set $A = 1/2$ and take α and r in the intervals $40^\circ \le \alpha \le 50^\circ$ and $0 \le r \le 0.5$. Considering all these parameter combinations, the maximum possible P is just 8.9% greater than the minimum possible value. Thus, $\rho(k)$ remains fairly invariant.[81]

Finally, for later convenience, we mention that in the limit of $r = 0$ and $\alpha = 45^\circ$ our billiard becomes the 45°–45° right triangle of sides $l_1 = l_2 = 1$, whose exact eigenfunctions and eigenwavenumbers are given by[82] (with $l \neq m$ positive integers)

$$\psi_{lm}(x,y) = \sin[l\pi\,x]\,\sin[m\pi\,y] - \sin[m\pi\,x]\,\sin[l\pi\,y],$$
$$k_{lm} = \pi\,\sqrt{l^2+m^2}. \tag{2}$$

Note that the above ψ_{lm} is an antisymmetric superposition of the square billiard solutions.

III. RESULTS

To explore how the k_n's vary with the geometric parameters of a billiard (here α and r), the procedure is direct. We fix one of the two parameters and set different values for the other, generically γ. For each γ, we obtain the corresponding eigenvalues, say, ranging from the n_i-th to the n_f-th level. In this way, for all $n_i \le n \le n_f$, we generate graphs (or "paths") representing the variation of k_n with γ. For some particular cases of interest, we also calculate and plot $|\psi_n(\mathbf{r})|^2$. As mentioned in Sec. I, these steps are relatively straightforward to implement using the BWM (for a full detailed description, see Ref. 78). Regarding numerical accuracy, the BWM has already been applied with other purposes to the quantum Sinai billiard in Ref. 77, yielding k_n's with typical error estimations around 0.04%—checked through distinct approaches. Once we use the same protocol, the numerical discretization method, and matrix sizes of Ref. 77, for the wavenumber intervals analyzed our results here have similar precision [e.g., one of our tests have been to compare the present simulations for the eigenwavenumbers and eigenstates of $\alpha = 45^\circ$ and $r = 0$ with the exact expressions in Eq. (2), finding remarkable agreement for the eigenstates and a difference of 0.04% and even less for the correct k_n's, Secs. III B and IV and Appendix B]. We finally mention that the accuracy of the BWM depends, as in any approach, on the discretization (number of points) taken on the billiard boundaries. Therefore, further details on such a procedure and how it relates to the obtained numerical precision are addressed in Appendix A.

We also observe that since we are discussing a totally desymmetrized Sinai billiard (when $r \neq 0$), the system should not present degeneracies unless for accidental ones.[83,84] Thus, the paths $k_n(\gamma)$ in most cases do not cross each other (but see an exception in Sec. III B). We further remark that the emergence of degeneracies as we change either α or r does not violate the von Neumann–Wigner theorem (refer to Refs. 71 and 85) because by varying just one of these parameters, we are in fact changing all the billiard sides [cf. Eq. (1)].

A. General trends when varying α

For $r = 0.2$ and $44^\circ \leq \alpha \leq 46^\circ$, a set of paths $k_n(\alpha)$'s are shown in Fig. 2. For $\alpha = 44^\circ$, we have $n_i = 152$ and $n_f = 177$ in Fig. 2(a) and $n_i = 357$ and $n_f = 397$ in Fig. 2(b). As it should be, $\Delta n/\Delta k$ increases with k_n. Indeed, compare the number of eigenwavenumbers in the k numerical interval 98–103, Fig. 2(b), with that for k in 65–70, Fig. 2(a). Notice also that for the present range for α, most of the k_n's do not suffer important deflections [the curves $k_n \times \alpha$ are fairly vertical lines, especially in Fig. 2(a)]. However, some k_n's in specific α regions go through considerable changes. Two examples of such regions are indicated by gray rectangles in Fig. 2 and are detailed in Figs. 3 and 4. In special, neighbor trajectories, $k_n(\alpha)$ and $k_{n+1}(\alpha)$, tend to repel each other if very close together, a behavior known as avoided crossing (AC). For instance, in Fig. 3, as α increases, we observe an initial approximation until a minimal separation and then a rapid splitting between paths d–e and g–h and paths h–i and k–l.

In Fig. 3, we show the gray region depicted in Fig. 2(a) and a few representative density plots of the eigenstates corresponding to the indicated (k_n, α) pair values. In all the density plots in this work, darker spots indicate higher values of $|\psi_n|^2$. For the sake of nomenclature, hereafter, we shall call a *branch* the segment of a given trajectory $k_n(\gamma)$, which is delimited by two successive ACs. Thus, the five paths (from left to right) seen in the first panel of Fig. 3 have, respectively, 1, 2, 3, 3, and 2 branches for $44^\circ \leq \alpha \leq 45.2^\circ$. As previously mentioned, there are levels that are not "perturbed" by the nearby states. An example is the path a–b–c in Fig. 3. In this case, the morphology of eigenfunctions (a)–(c) is very similar since the wavenumber variation is minimal and $\Delta\alpha$ is just 1.2°. Moreover, they did not display any particular pattern or spacial characteristic: the $|\psi_n|^2$ are uniformly and fairly randomly distributed (in terms of peaks and nodal lines) in accordance with Berry's conjecture.[31]

This behavior of a–b–c contrasts with the somehow correlated dynamics of d–e–f with g–h–i–j, g–h–i–j with k–l–m, and k–l–m with n–o. For instance, consider the paths d–e–f (representing level n) and g–h–i–j (level $n+1$). Leaving from $\alpha = 44^\circ$, they evolve toward each other until $\alpha \approx 44.26^\circ$, then going through a strong repulsion due to an AC. The morphology of the eigenfunctions at d of level n and g of level $n+1$ (both before the AC) is quite distinct. However, d (before the AC) and h of $n+1$ (after the AC)—as well as l of $n+2$—are akin. Likewise, for the shapes of the states, g and e (this latter belonging to the level n, located after the AC) display a reasonable resemblance. Finally, compare the states k and i with h and l, also l and o with n and m. In all these cases, succession of branches (say, labeled x, y, and z) of distinct paths form more or less straight line structures (denoted as xyz) along a certain extension of the $k \times \alpha$ space. In Fig. 3, they can be identified as dhlo (with the state o representing the end of the structure; after this, the corresponding branch starts to curve), gef and kij.

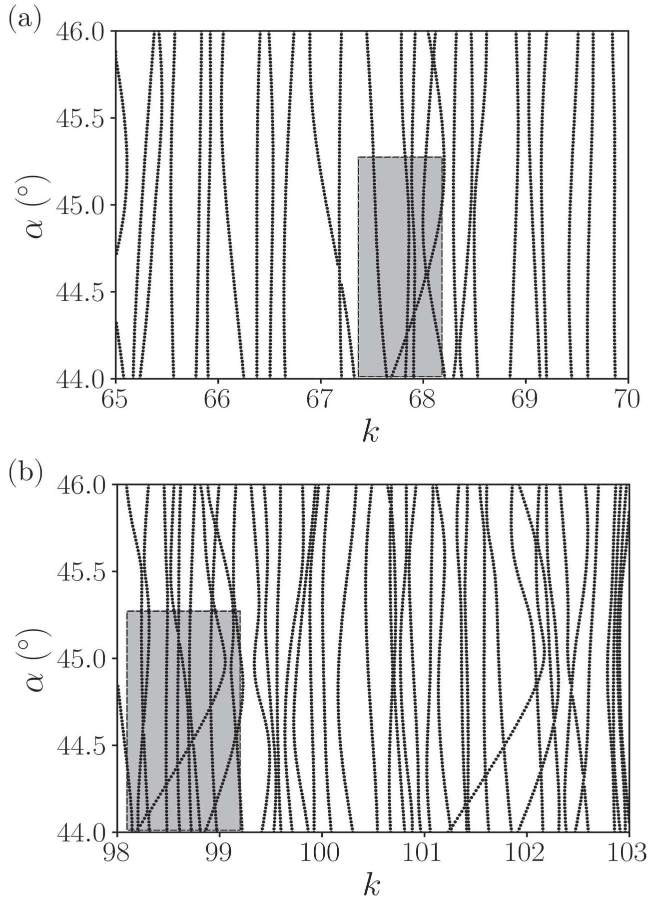

FIG. 2. For $r = 0.2$ and α varying from 44.0° to 46.0°, the corresponding $k_n(\alpha)$ for $n_i \leq n \leq n_f$ with (a) $n_i = 152$, $n_f = 177$ and (b) $n_i = 357$, $n_f = 397$ (in both cases, the values of n_i and n_f are relative to $\alpha = 44.0^\circ$). The gray regions are shown in detail, respectively, in Figs. 3 and 4.

The above phenomenology is also present in Fig. 4. However, in this higher k region of the spectrum, we have a greater number of ACs. Thus, the straight line-like structures tend to be composed of a larger number of branches. An example is adgjklm, whose eigenstates morphology are very similar. However, short line structures are also possible, such as nop (with the state p marking its end). Equally here, a kind of state morphology switching is observed along the trajectories $k_n(\alpha)$ and $k_{n+1}(\alpha)$ in the neighborhood of ACs. Indeed, compare in Fig. 4 the density plots (a) with (d) and (b) with (c); (d) with (g) and (e) with (f); and (g) with (j) and (i) with (h). The blowups in Fig. 4 illustrate detailed shapes of some ACs.

At this point, we shall summarize the results so far, putting them in a common framework (refer also to some extra material, complementing the present analysis, in Appendix B). Thus, suppose the paths n and $n+1$ displaying an AC at α_1, the paths $n+1$ and

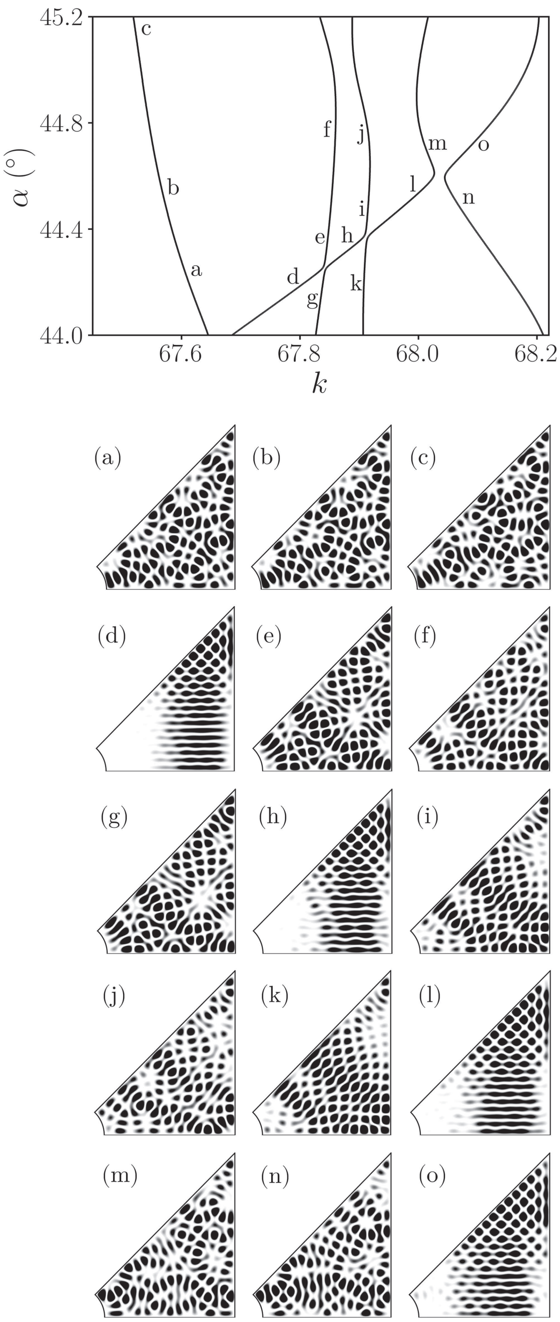

FIG. 3. The $k_n \times \alpha$ corresponding to the gray region in Fig. 2(a) as well as the $|\psi_n|^2$ for particular parameters values indicated as a, b, c, d, . . ., along the paths or trajectories $k_n(\alpha)$. Concretely: (a) $k = 67.5999$, $\alpha = 44.20°$; (b) $k = 67.5594$, $\alpha = 44.50°$; (c) $k = 67.5129$, $\alpha = 45.10°$; (d) $k = 67.7735$, $\alpha = 44.15°$; (e) $k = 67.8448$, $\alpha = 44.32°$; (f) $k = 67.8528$, $\alpha = 44.70°$; (g) $k = 67.8305$, $\alpha = 44.15°$; (h) $k = 67.8648$, $\alpha = 44.30°$; (i) $k = 67.9130$, $\alpha = 44.42°$; (j) $k = 67.9106$, $\alpha = 44.70°$; (k) $k = 67.9017$, $\alpha = 44.15°$; (l) $k = 67.9767$, $\alpha = 44.50°$; (m) $k = 68.0546$, $\alpha = 44.55°$; (n) $k = 68.1603$, $\alpha = 44.15°$; and (o) $k = 68.0772$, $\alpha = 44.70°$.

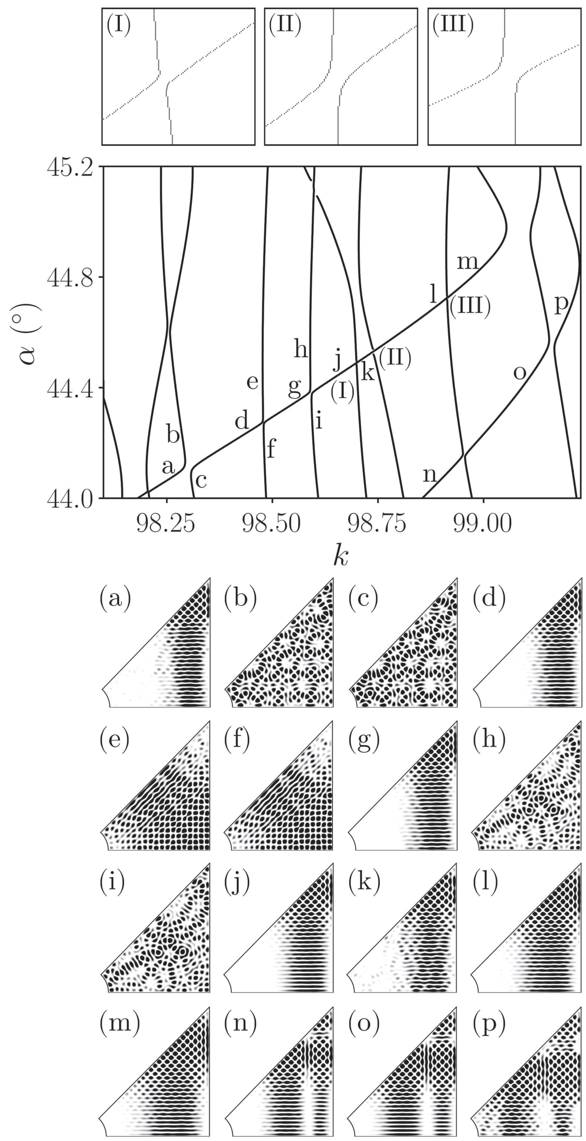

FIG. 4. The same as in Fig. 3, but for the gray region of Fig. 2(b). The blowups evidence very sharp avoided crossings. Parameters values: (a) $k = 98.2296$, $\alpha = 44.05°$; (b) $k = 98.2946$, $\alpha = 44.16°$; (c) $k = 98.3127$, $\alpha = 44.04°$; (d) $k = 98.4477$, $\alpha = 44.25°$; (e) $k = 98.4778$, $\alpha = 44.35°$; (f) $k = 98.4803$, $\alpha = 44.20°$; (g) $k = 98.5315$, $\alpha = 44.33°$; (h) $k = 98.5919$, $\alpha = 44.50°$; (i) $k = 98.5961$, $\alpha = 44.30°$; (j) $k = 98.6547$, $\alpha = 44.45°$; (k) $k = 98.7041$, $\alpha = 44.50°$; (l) $k = 98.8878$, $\alpha = 44.70°$; (m) $k = 98.9670$, $\alpha = 44.80°$; (n) $k = 98.8820$, $\alpha = 44.05°$; (o) $k = 99.0753$, $\alpha = 44.38°$; and (p) $k = 99.2017$, $\alpha = 44.70°$.

$n+2$ an AC at α_2, $n+2$ and $n+3$ at α_3, etc., with $\alpha_{i+1} > \alpha_i$. Furthermore, let us label as branch i that is associated with the path $n+i$ between α_i and α_{i+1}. If all these branches i interpolate a rather smooth curve (in the previous examples, straight lines; however, see Sec. III B), the eigenstates of the resulting formations do exhibit a same characteristic morphology. This is analogous to a soliton propagating in a given medium (in our case, the $k \times \gamma$ space) without any shape deformation. Moreover, such dynamics in the system geometric parameter space tends to induce an exchange between the eigenstate morphologies of neighbor paths (for the nature of such morphologies, see Sec. IV). In other words, along the aforementioned soliton-like structures, the typical pattern of ψ_n immediately after an AC becomes that of ψ_{n+1} immediately before this same AC and vice versa. As pointed out in Sec. I, solitons in the spectrum of quantum chaotic systems have been observed in the literature under different contexts.[61–65,68,71] As nicely outlined in Ref. 86, there are a few potential mechanisms justifying their existence.[65,66,69,70] We propose in Sec. IV that in our problem, very basic undulatory-geometric factors can explain these present findings.

B. General trends when varying *r*

In this section, we consider some specific values for the angle α and vary the radius r, investigating the resulting spectra soliton profiles.

In Fig. 5, we show the $k \times r$ families for $60 \leq k \leq 70$, $0 \leq r \leq 0.5$ and α is equal to (a) 44°, (b) 45°, and (c) 46°. First, from a direct visual inspection, it becomes clear that the solitons—recalling, branches interpolating smooth curves—no longer correspond only to straight lines (the explanation for so is left to Sec. IV). Second, there are considerably longer soliton-like structures than in Sec. III A. To understand this latter fact, recall that in Sec. III A, we have considered $40° \leq \alpha \leq 50°$, so just about 11% of the full range $0° \leq \alpha \leq 90°$. On the other hand, for $A = 1/2$, the side l_1 (Fig. 1) can vary from 1 to 0 for r between 0 and $1/\sqrt{1-(\pi/2-\alpha)\tan[\alpha]}$ [Eq. (1)]. Thus, for $44° \leq \alpha \leq 46°$, $0 \leq r \leq 0.5$ represents approximately 23% of the maximum possible variation of r. Moreover, for $\alpha > 45°$, the soliton-like structures in the $k \times \alpha$ space tend to be destroyed as r increases (e.g., compare the three graphs in Fig. 12 of Appendix B). Also, we have numerically checked that the same is true when $\alpha < 30°$. Then, for $r = 0$, a "contiguous" $k \times \alpha$ soliton is restricted to 45°–60° (having a specular image in the region 30°–45°). The angles of 60° and 30°, therefore, act as separatrices or borders for the solitons since they correspond to integrable billiards (the rich soliton patterns for right triangle billiards will be explored in a dedicated future contribution).

A relevant dynamics perceived from Fig. 5 is how the families of states of the desymmetrized Sinai billiard ($r \neq 0$) emerge from the right triangle billiard ($r = 0$) states. For the considered interval for k, we have $0.089 < \lambda < 0.105$. Then, for $r < 0.044$ ($\approx \overline{\lambda}/2$), the families are fairly vertical lines, indicating that up to such a radius value and a wavelength range, the Sinai ψ_n's are basically weak perturbations of the triangle ones. In other words, the desymmetrized Sinai states can be considered, in a first approximation, deformations of the right triangle states for r is small. We also see that there are no new quantum levels arising in the k vs $r > 0$ regions; only certain replicated trajectories [i.e., coinciding $k_n(r)$'s] at $r = 0$ get separated after some $r > 0$. In fact, this should be expected from the restrictions imposed on the billiards, i.e., fixed area $A = 1/2$ and just a small change in the perimeter P. For instance, from Fig. 5(b) (for the $\alpha = 45°$ case), as we increase r, we notice splittings of double and triple degeneracies remnant ("memory") of the 90°–45°–45° triangular billiard.

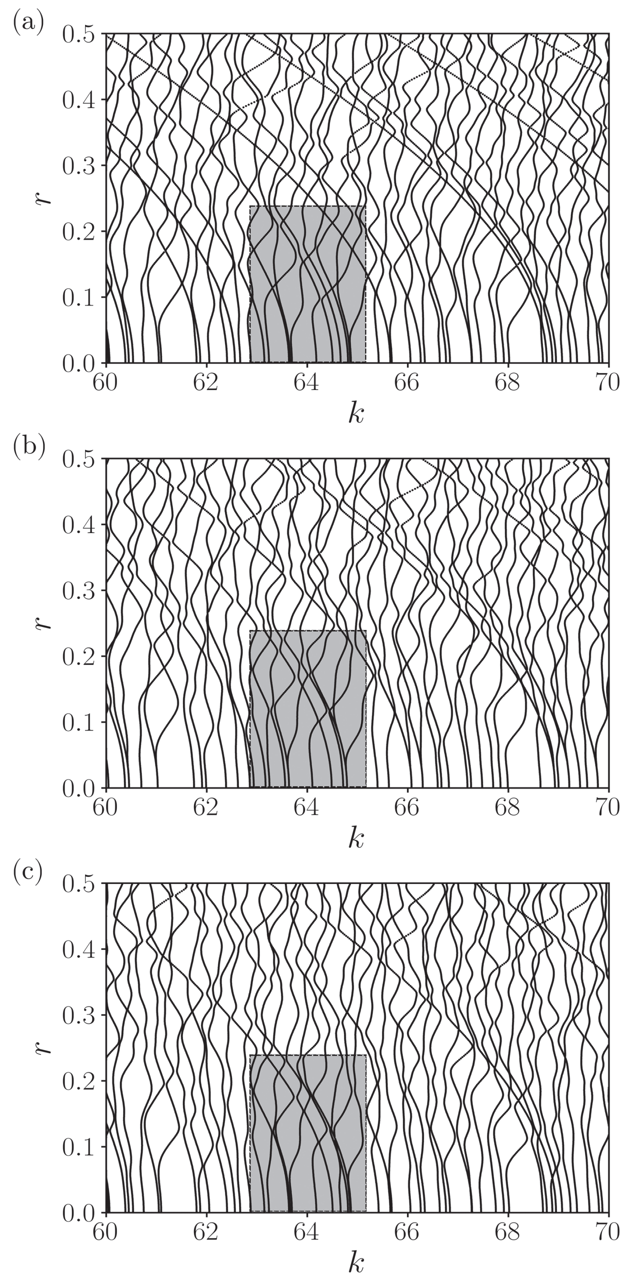

FIG. 5. Similar to Fig. 2, but for three fixed values of α: (a) $\alpha = 44.0°$, (b) $\alpha = 45.0°$, (c) $\alpha = 46.0°$, and r varying from 0 to 0.5. Here, the levels range from $n_i = 129$ to $n_f = 177$ (for $r = 0.0$). The gray regions are shown in detail in Figs. 6–8.

Specific regions of Figs. 5(a)–5(c) (corresponding to more rounded parts of the soliton-like structures) are shown in detail, respectively, in Figs. 6–8. As in Sec. III A, the solitons also have distinct lengths (although, as previously discussed, usually longer than those from $\{k_n(\alpha)\}$). For example, in Fig. 6, if we overlook the step-like segment from d to e, the "single" soliton abcde is longer than fghi and jkl. The state morphologies along a-e, including e, are all similar with the exception of d [compare the plots (a)–(e) in Fig. 6]. Actually, the state at d seems to be disturbed by the nearby trajectory c–i. However, once c–i runs away from d–e as r increases, the morphology of the states at the end of the soliton abcde, like e, becomes again similar to those at its initial part, stretch abc. Conversely, when contrasted to (f), (g), and (h), the state (i) in Fig. 6—terminating the soliton fghi—presents a distorted pattern due to its proximity to the path d–e. Last, for jkl, the state in l displays some deviation from j and k [see (j)–(l) in Fig. 6] since l is located at the soliton ending.

The breakdown of degeneracies is very apparent in Fig. 7 for $\alpha = 45°$. For instance, for $r = 0$, we have three degenerated states in j, whose numerically obtained $|\psi_n|^2$'s are shown in (j_1), (j_2), and (j_3). They correspond, respectively, to the following quantum numbers l, m in Eq. (2): 5, 20; 8, 19, and 13, 16, as one can easily check by plotting the associated ψ_{lm}'s. The exact wavenumber is $k_{lm} = 64.76559\ldots$, thence with a difference of only 0.03% for $k = 64.7857$ in j. As r raises, one of these three states splits (around $r \approx 0.044$) giving place to the path j–m. As the billiard radius r further increases, the other two states, about $r \approx 0.09$, also separate, leading to the trajectories j–l and j–k. In particular, observe that the morphologies of the states at k, l, and m (for $r \neq 0$) are very distinct from those at j (for $r = 0$), Figs. 7 (j_1), (j_2), (j_3), (k), (l), and (m). For this $\alpha = 45°$ family of billiards, we again observe both long, abcde, and very short soliton-like structures, e.g., kn and hi.

In our desymmetrized Sinai billiard, even for the $\alpha = 45°$ case, there are no (apparent) specific symmetries for the system. Therefore, eventual degeneracies should be accidental.[83–85] In this regard, we mention that such kind of degeneracy has already been observed for two coupled Sinai billiards[87] as well as for the bound states in the continuum of an open Sinai billiard.[88] Moreover, we recall from the discussion just before Sec. III A that in the present case, we have a finite probability of (accidental) degeneracies since by varying γ (here r), in fact, we are also changing the billiard sides (to keep the area constant); consequently, we are adjusting more than one shape parameter. In Fig. 7, the detail indicates that the region marked as I is indeed a crossing, yielding a twofold degeneracy. The analysis of the $k \times r$ space in terms of trajectories allows a simple heuristic explanation for it. Nearby region I, there are two strong ACs and four very close trajectories, a–b–o–h, f–g–p, j–k–n, and j–l, the latter two consequence of the threefold degeneracy eigenstates at j, which are broken as r increases. Hence, there is not enough room for the middle paths to evolve without at least one collision between them: a–b–o–h repels f–g–p toward j–k–n, which by its turn is repelled away from j–l against f–g–p, making the crossing unavoidable. Certainly, this is just a qualitative argument, and further quantitative investigation might be in order. However, this already could point that in some instances, accidental degeneracy can be due to the inevitability of colliding trajectories in the *energy* × *parameters* space.

A mixing of the behavior in Figs. 6 ($\alpha = 44°$) and 7 ($\alpha = 45°$) is replicated in Fig. 8 ($\alpha = 46°$). For instance, as in Fig. 6, there are no degeneracies for $r = 0$ in Fig. 8. On the other hand, similarly to some paths in Fig. 7, as r increases from zero, the paths in Fig. 8 originated from f, g, l, and o develop intricate interactions when close together. In fact, there is an extremely narrow AC between f–i and g–h, whereas the trajectories l–m and g–h do cross (details are not shown), leading to a degeneracy at $k \approx 64.546$ and $r \approx 0.113$. Finally, for the features of the soliton abcde of Fig. 8 along its straight line path, see Appendix C.

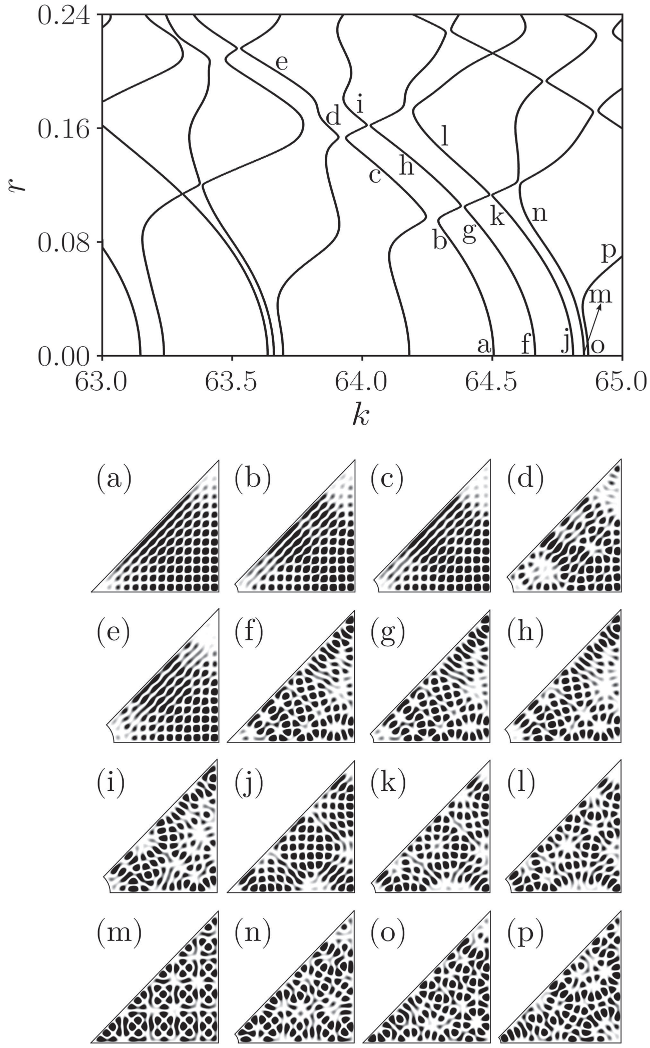

FIG. 6. Details of the gray region of Fig. 5(a), where $\alpha = 44.0°$. The parameter values are (a) $k = 64.5051$, $r = 0.0$; (b) $k = 64.3278$, $r = 0.084$; (c) $k = 64.0864$, $r = 0.129$; (d) $k = 63.8769$, $r = 0.16$; (e) $k = 63.6349$, $r = 0.187$; (f) $k = 64.6642$, $r = 0.0$; (g) $k = 64.4572$, $r = 0.09$; (h) $k = 64.1936$, $r = 0.138$; (i) $k = 63.9751$, $r = 0.169$; (j) $k = 64.8100$, $r = 0.0$; (k) $k = 64.5515$, $r = 0.102$; (l) $k = 64.4546$, $r = 0.12$; (m) $k = 64.8520$, $r = 0.0$; (n) $k = 64.7634$, $r = 0.06$; (o) $k = 64.8683$, $r = 0.0$; and (p) $k = 64.9230$, $r = 0.058$.

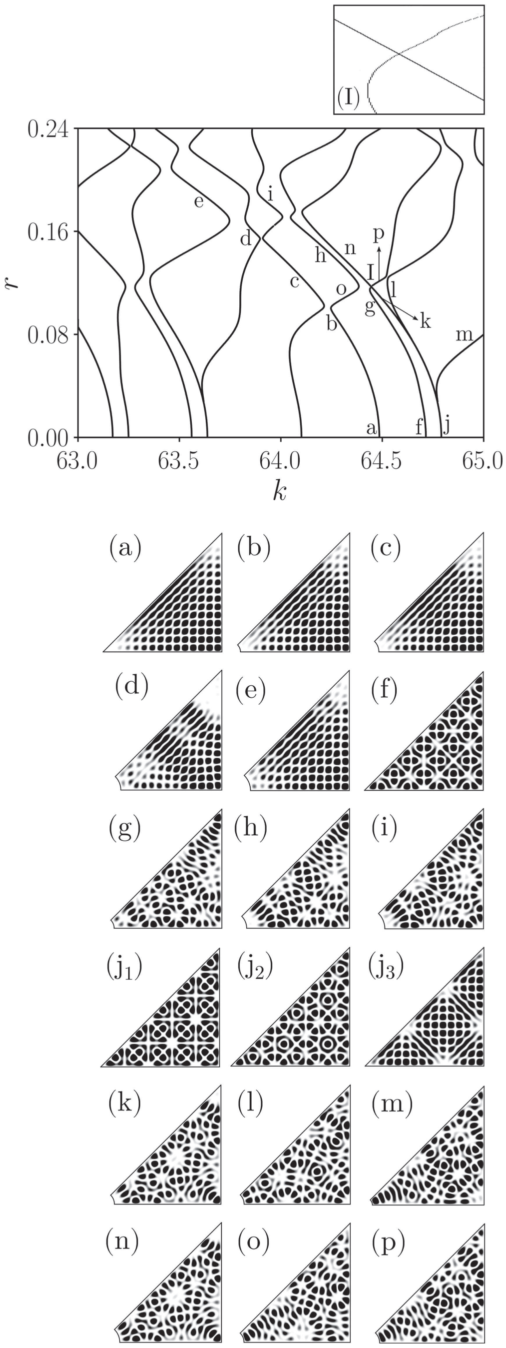

FIG. 7. Details of the gray region of Fig. 5(b), where $\alpha = 45.0°$. The parameter values are (a) $k = 64.4804$, $r = 0.0$; (b) $k = 64.3089$, $r = 0.083$; (c) $k = 64.0927$, $r = 0.125$; (d) $k = 63.8601$, $r = 0.16$; (e) $k = 63.6719$, $r = 0.181$; (f) $k = 64.7097$, $r = 0.0$; (g) $k = 64.5019$, $r = 0.097$; (h) $k = 64.2425$, $r = 0.142$; (i) $k = 63.9308$, $r = 0.182$; (j) $k = 64.7857$, $r = 0.0$; (k) $k = 64.4911$, $r = 0.108$; (l) $k = 64.5263$, $r = 0.111$; (m) $k = 64.8407$, $r = 0.061$; (n) $k = 64.2125$, $r = 0.153$; (o) $k = 64.3304$, $r = 0.11$; and (p) $k = 64.4965$, $r = 0.1224$.

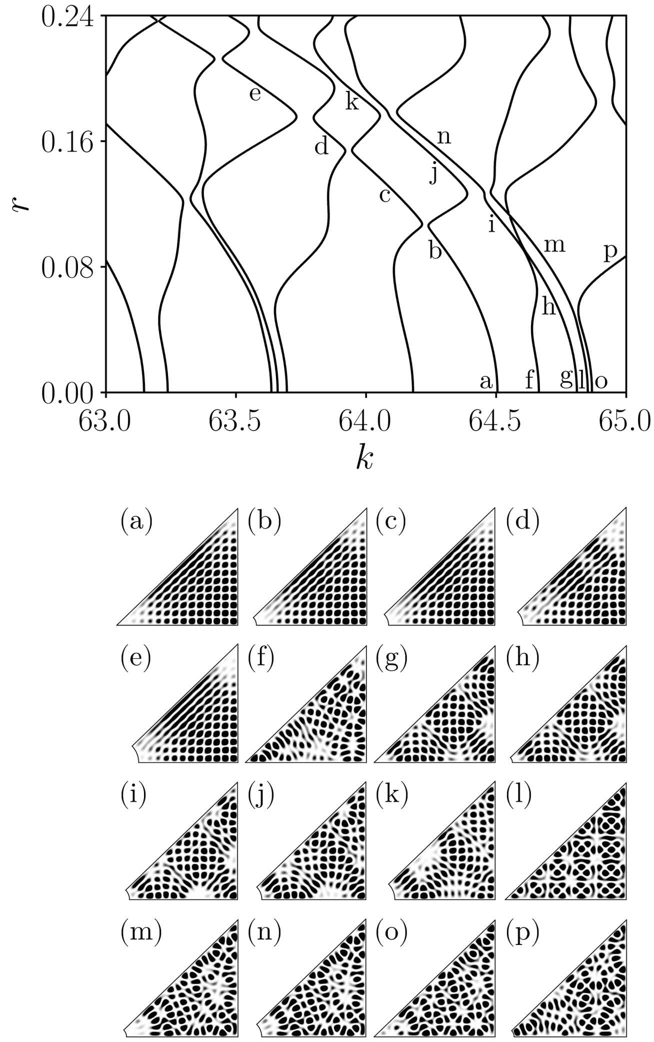

FIG. 8. Details of the gray region of Fig. 5(c), where $\alpha = 46.0°$. The parameter values are (a) $k = 64.5049$, $r = 0.0$; (b) $k = 64.2943$, $r = 0.093$; (c) $k = 64.0881$, $r = 0.131$; (d) $k = 63.8871$, $r = 0.16$; (e) $k = 63.5579$, $r = 0.199$; (f) $k = 64.6642$, $r = 0.0$; (g) $k = 64.8100$, $r = 0.0$; (h) $k = 64.7206$, $r = 0.06$; (i) $k = 64.4905$, $r = 0.115$; (j) $k = 64.2475$, $r = 0.152$; (k) $k = 63.9808$, $r = 0.188$; (l) $k = 64.8519$, $r = 0.0$; (m) $k = 64.6945$, $r = 0.083$; (n) $k = 64.3062$, $r = 0.151$; (o) $k = 64.8683$, $r = 0.0$; and (p) $k = 64.9034$, $r = 0.075$.

IV. DISCUSSION

Before finally addressing the mechanisms underlying the observed families of solitons, we shall consider two relevant aspects of the problem.

The first is to illustrate our billiards dynamical character through the nearest-neighbor $P(s)$ statistics.[2] Given that classically, the Sinai billiard is hyperbolic[20,22,89] for any $r \neq 0$, in the quantum case, $P(s)$ should be given by the Wigner–Dyson distribution.[33,79] However, as discussed in Sec. III A, for $r = 0$, we have right triangle billiards, and thus, in principle, $P(s)$ must interpolate between the

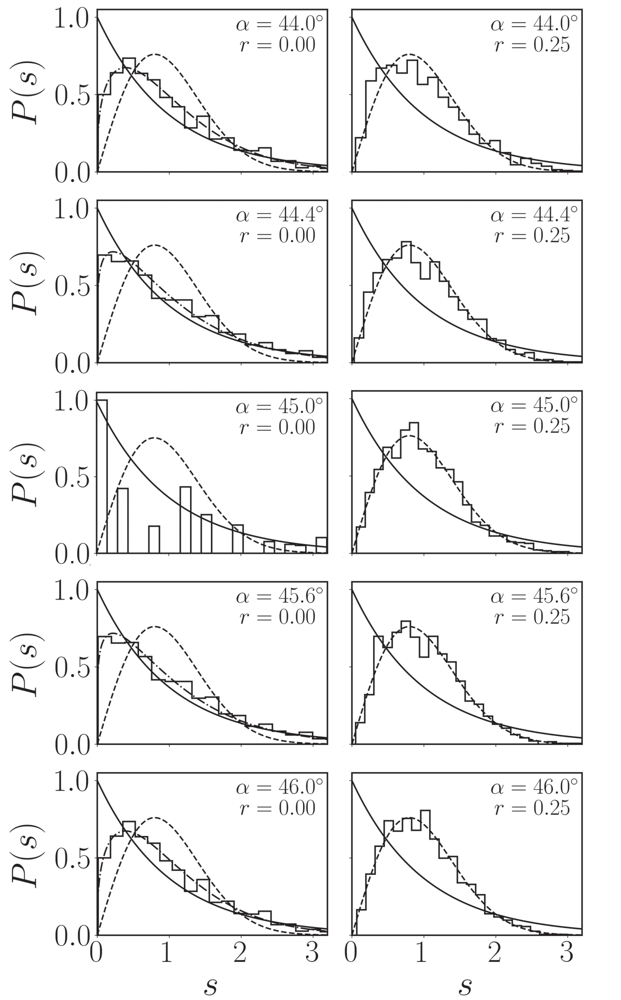

FIG. 9. The numerical nearest-neighbor level spacing statistics $P(s)$ (staircase plots) for $r = 0.0$ and $r = 0.25$ and different values of α, considering 10^4 levels for $\alpha = 45.0^\circ$ and 1530 levels otherwise. The Poisson, Wigner–Dyson, and Brody [Eq. (3)] distributions are represented, respectively, by continuous, dashed, and dotted–dashed curves. The Brody fittings for $r = 0.0$ are obtained from $q = 0.339\,07$ ($\alpha = 44.0^\circ$), $q = 0.182\,65$ ($\alpha = 44.4^\circ$), $q = 0.182\,65$ ($\alpha = 45.6^\circ$), and $q = 0.339\,07$ ($\alpha = 46.0^\circ$).

Poisson and Wigner–Dyson functional forms (with the exception of our integrable[82,90] 45°–45° and 30°–60° cases). Therefore, for $r = 0$, we use as a fitting model the Brody distribution[91] (with $\Gamma[\cdot]$ the Gamma function)

$$P(s) = \frac{q+1}{s}\left(\Gamma\left[\frac{q+2}{q+1}\right]s\right)^{q+1}\exp\left[-\left(\Gamma\left[\frac{q+2}{q+1}\right]s\right)^{q+1}\right], \tag{3}$$

leading to the Poisson (Wigner–Dyson) expression when $q = 0$ ($q = 1$). For $r = 0$ and $r = 0.25$, results for some α's are depicted in Fig. 9. As expected, for $r = 0.25$, the Wigner–Dyson distribution describes very well the calculated $P(s)$. On the other hand, for $r = 0$,

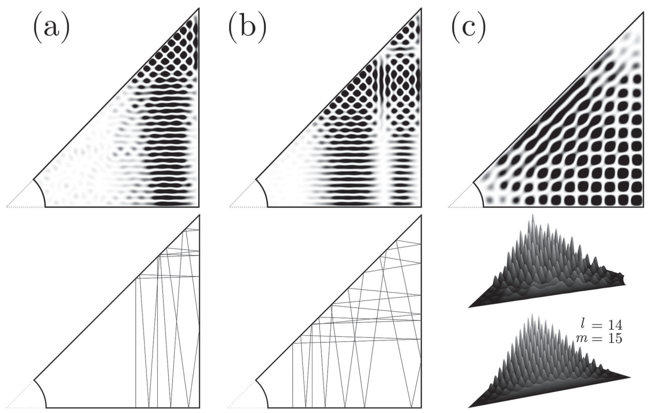

FIG. 10. The upper row displays the density plots for (a) the state (a) in Fig. 4 (corresponding to $r = 0.2$ and $\alpha = 44.05^\circ$), (b) the state (n) in Fig. 4 (also corresponding to $r = 0.2$ and $\alpha = 44.05^\circ$), and (c) the state (e) in Fig. 7 ($r = 0.181$ and $\alpha = 45.0^\circ$). For this latter, a 3D graph is also presented, whose shape pattern is very similar to $|\psi_{14\ 15}|^2$ of Eq. (2), bottom of column (c). The states in (a) and (b) are the scarred eigenstates of the two shown classical orbits.

the Brody distribution with different values of q yields good fittings for the distinct α's. The exception is the integrable $\alpha = 45^\circ$ billiard, whose $P(s)$ agrees with that in Ref. 82.

The second is to outline important facts about classical periodic orbits in arbitrary right triangle billiards (aRTB). We recall that in billiards possessing parallel borders, the standard definition of (marginally stable) bouncing ball BB orbits is back and forth collisions—always at an incidence of 90°—between two parallel sides of the billiard, e.g., between the up and down sides of the rectangular part of the stadium.[74] Of course, from such a definition, we cannot have BB for right triangles since they have no parallel sides. However, in the particular case of a 45°–45° right triangle, somewhat similar to a BB is a periodic orbit in which a particle leaving normally from one cathetus hits the hypotenuse and then goes immediately toward the second cathetus also at a right angle. Furthermore, for aRTB, almost all orbits that start perpendicular to one cathetus will be periodic,[92] although the periods may be very long. We are not aware of related theorems for trajectories leaving perpendicularly to the hypotenuse. In fact, we have performed various numerical simulations, and for arbitrary α, this does not seem to be usually the case (nonetheless, long periodic orbits do arise for very fine tuning starting positions on the hypotenuse). However, when departing normally from the hypotenuse hitting one cathetus, if the subsequent collision is with the other cathetus, then necessarily such a path will be periodic (of period 6). Last, a rigorous proof shows[93] that any periodic orbit for aRTB is unstable. This is exactly the kind of orbit associated with quantum scars.

From the results in Sec. III, we can identify certain recurrent behavior for the soliton-like structures in the desymmetrized Sinai billiard. Some of these trends have already been observed in the literature for distinct systems—see Sec. I—and are indicated below as (A), (B), and (E1). The others, (C), (D), and (E2), although corresponding to known properties, to the best of our knowledge, have not been fully explored in the present spectra

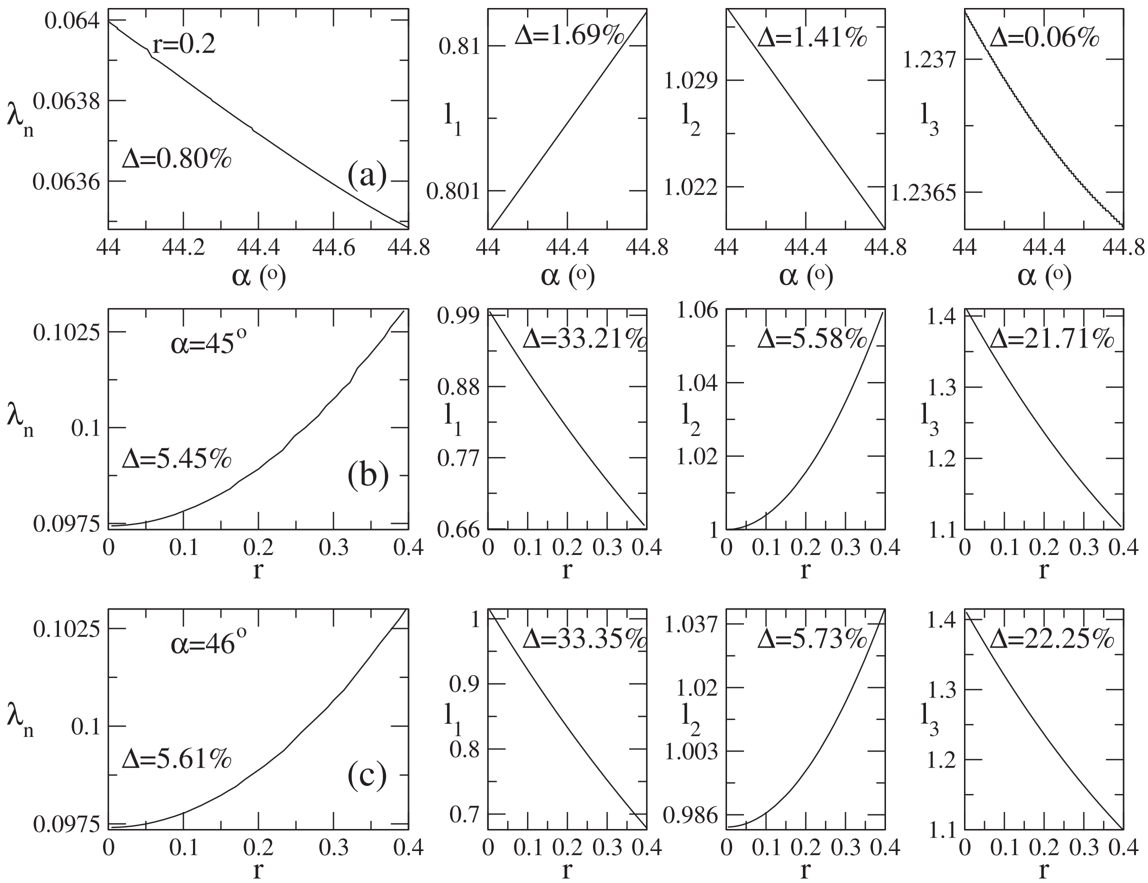

FIG. 11. In each row, the eigenstate wavelength λ_n and the corresponding Sinai billiard sides l_1, l_2, and l_3 as a function of the geometric parameter γ (either α or r) along the soliton structures: (a) adgjklm of Fig. 4, (b) abcde . . . of Fig. 7 (see also Fig. 5), and (c) abcdeqrs of Fig. 14 in Appendix C. Overall, $\lambda_n(\gamma)$ tends to follow the same behavior of the billiard side $l_2(\gamma)$. The parameter Δ represents the % difference between the highest and lowest ordinate values in each plot.

soliton context. If viewed as effective "single" structures (or curves), (A) the solitons are much less sinuous than the individual trajectories $k_n(\gamma)$'s, consequently reducing the overall path curvatures. (B) For a given geometric parameter variation $\Delta\gamma$, the change Δk is higher along a soliton than along each $k_n(\gamma)$'s. (C1) Regarding the ψ_n's, those associated with a given soliton have very similar morphologies. (C2) Moreover, they can be more (e.g., Figs. 3 d–h–l–o, 4 a–d–g–j–k–l–m, and 4 n–o–p) or less [e.g., Fig. 8 a–b–c–d–e] spatially localized. Nonetheless, they tend to present low amplitudes in the neighborhood of the billiard arc of a circle corner. (D) There is a sort of morphology switching between states of neighbor paths across the ACs of a soliton. For instance, observe the correspondences d$\sim$h and g$\sim$e along the trajectories d–e and g–h in Fig. 3 and i$\sim$h and g$\sim$j along g–h and i–j in Fig. 4. It is exactly such type of dynamics that seems to prompt (C1). Finally, the soliton states are either (E1) associated with akin scars of the RTB unstable periodic orbits or (E2) correspond to *memory* states, i.e., ψ_n's, which maintain the basic shape pattern of a suitable state of the RTB as γ varies. In both instances, the ψ_n's morphologies are preserved as the billiard geometry changes by means of the corresponding rescaling of k_n or equivalently of λ_n (see below).

To clarify (E) above, we display in Fig. 10 the density plots of $|\psi_n|^2$'s for representative states of the solitons adgjklm and nop of Fig. 4 and abcde of Fig. 7. Regarding (E1), the states (a) and (b) in Fig. 10 are clearly much more concentrated in the right portion of the billiard, closer to the vertical side l_2. Therefore, intuitively speaking, these states would not "feel" the (wave) dispersing influence of the arc of the circle corner of the Sinai billiard.[22] So, being scarred states of orbits that do not visit the region near $\widehat{s}$, Fig. 1, or indistinguishable the same orbits for the related ($r = 0$) RTB. Actually, the shown classical periodic orbits for the $\alpha = 44.05^\circ$, cathetus lengths $l_1 + r$, l_2, and hypotenuse $l_3 + r$ RTB corroborate such a picture. We observe that the two periodic orbits in Fig. 10 correspond to the situation in which some collisions are normal[92] to the horizontal cathetus.

The previous argument, however, does not hold for the state (c) in Fig. 10 [which is (e) in Fig. 7]. Note that the family abcde starts at the state (a) in Fig. 7, which is an eigenstate of the integrable 45°–45° RTB. For this case, our calculated $k = 64.4804$ differs only by 0.032% of $k_{14\,15} = 64.4601$. A 3D plot of the exact $|\psi_{14\,15}|^2$ in Eq. (2) is depicted in Fig. 10 (although not shown, the numerically obtained wavefunction (a) in Fig. 7 matches almost perfectly $\psi_{14\,15}$). The emerging interference pattern of this $l = 14$, $m = 15$ mode makes $|\psi_{14\,15}|^2$ to be very small in a considerable region around the two acute angles. This key characteristic as well as the overall morphology of the states along the soliton abcde are very similar to $|\psi_{14\,15}|^2$, as we clearly see from the 3D plots in Fig. 10 and also from Fig. 7. Away from the acute angle regions, the plots evidence a well distributed pattern for the ψ's, but for local maxima of different heights, with higher (lower) peaks closer to the 90° angle (hypotenuse). This is not a typical conformation of scarred states, especially considering that one of these ψ_n's (at a) corresponds to an integrable billiard.

The above features are not just due to a particularity of the $\alpha = 45°$ billiard. The same qualitative characteristics are likewise found for $\alpha = 46°$ in Fig. 8 and in Fig. 14 of Appendix C (particularly, see the long soliton abcdeqrs), as well as for $\alpha = 44°$ in Fig. 6. For example, we have checked that a 3D plot of the state (a) in Fig. 8 has a good resemblance to the 3D plot of $|\psi_{14\,15}|^2$ in Fig. 10 (note also that they have very close k values). Therefore, across the soliton-like structures, ψ_n's retain memory of the "initial" $\psi_n|_{r=0}$ morphology—in our studies corresponding to integrable or pseudointegrable (for the 46°–44° case, the genus[10] is 22) RTBs. Furthermore, typically, a $\psi_n|_{r=0}$ originating a soliton vanishes around the RTB α and β angles [or at least around β, e.g., (f) in Fig. 6 and the soliton fghi]. This guarantees that ψ_n's of a similar shape can be accommodated into the desymmetrized Sinai billiard without a strong perturbation caused by $r > 0$.

As a last analysis, in all the examples considered (both for scarred and memory states), as we change a geometric parameter γ, the ψ_n's along the soliton-like structures preserve their general morphologies through a simple spatial rescaling within the modified billiards. In principle, it should create a correlation between the eigenstate wavelengths $\lambda_n = 2\pi/k_n$ and the billiard spatial dimensions. To verify this, we consider the λ_n's along the solitons adgjklm of Fig. 4, abcde ... of Fig. 7 (cf. Fig. 5) and abcdeqrs of Fig. 14. Such λ_n's and sides l_1, l_2, and l_3 of the associated Sinai billiards are shown in Fig. 11. We observe a good agreement between the variation of λ_n and the length l_2 of the vertical cathetus as γ (either α or r) varies. A certain discrepancy for the parameter Δ (see its definition in the caption of Fig. 11) is found for the soliton adgjklm of Fig. 4. In this case, $\Delta\lambda_n = 0.80\% < \Delta l_2 = 1.41\%$ for α ranging from 44° to 44.8°. Nonetheless, this is easily accounted for by noticing from the corresponding plots in Fig. 4 that the ψ_n's along the adgjklm structure also suffer a small broadening in the horizontal direction as α increases.

We end this section by comment on a remark made by one of the anonymous referees. Some of the examples in this contribution are bordering on the diffractive limit (the full limit would be achieved for $\lambda = 2\pi/k$ large compared to r). One possible illustration is (p) in Fig. 6, however, which is not associated with a soliton-like structure. Actually, the particular soliton states that we have examined more carefully here tend to display small amplitudes in the region very close to Sinai's arc of circle. Thus, somehow, they are not influenced by the billiards' circular boundary. To investigate parameter values for which diffraction effects become important for the present family of systems is certainly an interesting topic for further work. Nonetheless, if related to solitons, the ψ_n's resulting from diffraction most likely would be scarring states.

V. FINAL REMARKS AND CONCLUSION

In the present contribution, we have discussed a relevant quantum chaotic problem, the desymmetrized Sinai table. We have considered geometric parameters γ, determining the exact form of the billiard and whose change generates a whole family of systems. As pointed out in Sec. I, many interesting works in the literature examine universal features in the spectra of chaotic billiards as these γ vary. However, here, we have struck in a different direction, studying the particularities of soliton-like structures in the spectra of our billiards. These structures tend to result in non-general properties once their proliferation, exact shapes, lengths, etc., are often system-dependent. However, interestingly, the associated $\{\psi_n\}$ and $\{k_n\}$ along a given soliton share common characteristics, creating a kind of interrelationship among a fraction of the full set of eigenstates and eigenwavenumbers (or eigenenergies) of the full family.

More concretely, we have performed a detailed analysis of the mentioned $\{\psi_n\}$ and $\{k_n\}$ vs γ, unveiling (1) the states morphologic characteristics as well as (2) the geometric features of the billiard borders, which allow the solitons emergence. Regarding (1), perhaps it is a bit surprising that not only BB modes and scarred wavefunctions contribute to $\{\psi_n\}$. Indeed, eigenstates that we have called "memory" states, i.e., ψ_n's maintaining the localized shape patterns of particular solutions of integrable or pseudointegrable billiards (the case when γ assumes some special value, say γ_0), can also account for the soliton structures.

Given the previous observations, a natural question is whether or not our findings for the Sinai could extend to other billiards. Obviously, a definitive answer should demand the survey of an extensive number of distinct systems. Nevertheless, some general considerations can be put forward. For the sake of argument, suppose the billiard domain is written as $\Omega = \Omega_I \cup \Omega_{II}$, with Ω_I and Ω_{II} adjacent regions separated by the surface $\mathscr{S}$. Moreover, assume Ω_X $(X = I, II)$ delimited by $\mathscr{S} \cup \partial_X\Omega$, where $\partial\Omega = \partial_I\Omega \cup \partial_{II}\Omega$.

A first key factor is the existence of eigenstates whose specific morphologies are easily adaptable to the billiard contour $\partial\Omega$ for a continuous variation of γ. The change of γ might cause considerable modifications in $\partial_I\Omega$, but only a smooth adjustment of $\partial_{II}\Omega$, e.g., leading to a simple rescaling of a characteristic length size l of Ω_{II} such that $l(\gamma)$ is a well-behaved function. In this case, an eigenstate ψ_n localized in the region Ω_{II} would survive to the billiard deformation by just changing λ_n accordingly, i.e., for $\lambda_n(\gamma) \sim l(\lambda)$. This is analogous to what takes place in a quantum adiabatic process.

The second key factor is the existence of such proper localized ψ_n's for some particular billiard in the family, namely, when $\gamma = \gamma_0$. If for this γ_0 the billiard is already chaotic, the clear candidates are mostly BB modes and in a lesser degree scarred states (for very elucidating analysis in the quantum chaotic case, see, e.g., Refs. 65–70). However, we have shown for the desymmetrized Sinai that if for γ_0 the billiard is integrable or pseudointegrable, some of its specific ψ_n's with the right morphologies—and not related to BBs or scarring—can likewise contribute to the formation of the solitons. Conceivably, this also could take place for other tables, such as for polygon billiards with pockets (i.e., some corners substituted by small circles).[94]

Finally, it may be a great challenge to foresee the above phenomenology in a specific problem without exploring its energy spectrum for diverse γ's. However, if the above framework of setting $\Omega = \Omega_I \cup \Omega_{II}$ is possible, conditions for the occurrence of soliton-like structures eventually could be established from Bogomolny's quantum surface section method[95–98] e.g., considering $\mathscr{S}$. For sure, this is a compelling research agenda for future works focusing solitons in the spectrum of quantum chaotic billiards.

ACKNOWLEDGMENTS

We would like to thank a research grant from CNPq 304532/2019-3 (M. G. E. da Luz) and scholarships from CNPq (M. R. Sales) and Capes (A. L. Azevedo and F. Teston). We should also mention that the very stimulating and fruitful environment in the conference "Semiclassical Methods in Quantum Physics and Applications," held at the IIP-Natal, Brazil in 2019, strongly motivated some of the ideas in the present work.

AUTHOR DECLARATIONS

Conflict of Interest

The authors declare that there is no conflict of interest.

Author Contributions

M.R.S. and A.L.A. contributed equally to this work.

APPENDIX A: DETAILS ON THE BILLIARD BOUNDARY NUMERICAL DISCRETIZATION

We start observing that a great advantage of the present family of systems is that we can benchmark the discretization procedure by "probing" the integrable case, namely, the right 45°–45° triangle. Thus, for k around 105 (the maximum value in this work), we have computed the numerical eigenvalues for distinct discretizations and compared with the analytic ones, Eq. (2), until getting satisfactory results. Then, for the other cases, we have employed the same settings, i.e., the same number of points by a perimeter length unit along the billiard boundaries.

Our protocol was to consider $\Delta/\lambda = b$, where Δ is the perimeter length along the billiard border between two successive discrete points, $\lambda = 2\pi/k$, and b the parameter to control the method precision. The numerically determined good compromise values for $b = \overline{b}$ were $\overline{b}_s = 0.05$ and $\overline{b}_c = 0.025$, respectively, in the straight and circular parts of the billiards. For representative avoided crossings—such as (I)–(III) in Fig. 4—we repeated the calculations using $\overline{b}/2$ so as to double check their correct separations. Furthermore, for some extreme situations, as the crossing (I) in Fig. 7, we have used the somehow computationally expensive value of $\overline{b}/3$, confirming the qualitative results obtained with $\overline{b}$.

As a final extra test, which of course does not show if individual eigenstates present good numerical precision, but at least indicates whether or not one is missing a reasonable number of very closed k_n's, for non-integrable billiards and $\overline{b}$, we have confronted the number of k_n's up to a certain k with the usual Weyl formula. In all the wavenumber intervals examined, the agreement has been rather satisfactory. All these analyses have shown that for the phenomenology studied here, the BWM numerical accuracy was enough for our purposes.

APPENDIX B: SOME EXTRA RESULTS BY VARYING α

Figure 12 shows $k_n \times \alpha$ in the range $40^\circ \leq \alpha \leq 50^\circ$ and $60 \leq k \leq 70$ for three different values of the radius r: (a) $r = 0$, (b)

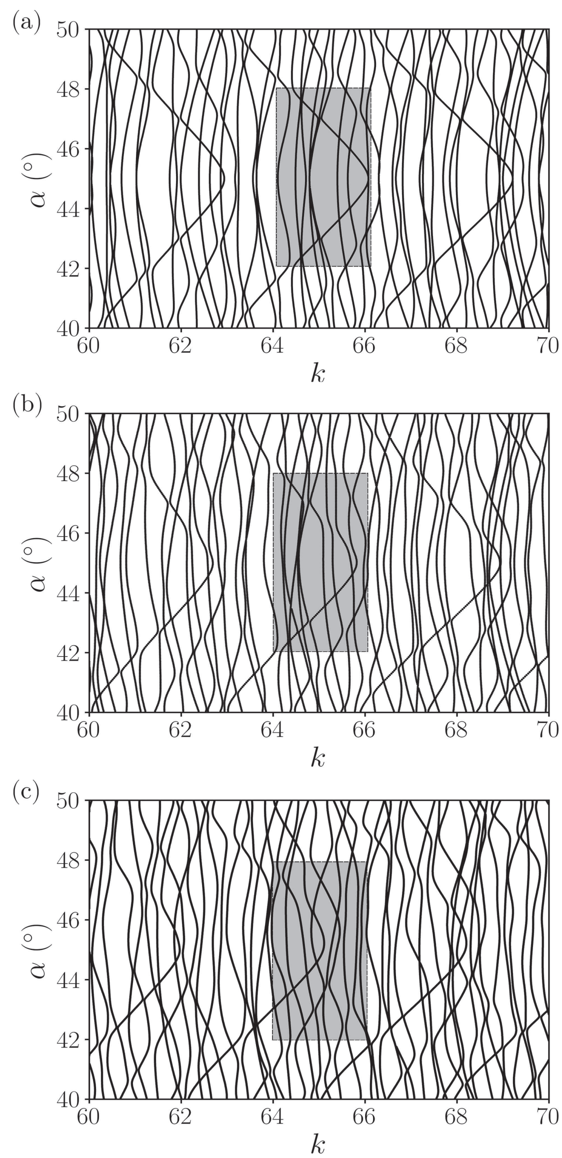

FIG. 12. Similar to Fig. 2, but for (a) $r = 0.0$ and $n_i = 128$, $n_f = 177$, (b) $r = 0.1$ and $n_i = 128$, $n_f = 177$, (c) $r = 0.2$ and $n_1 = 129$, $n_f = 177$; all n's are taken as reference $\alpha = 40.0^\circ$. The gray regions are shown in detail in Fig. 13.

$r = 0.1$, and (c) $r = 0.2$ (the latter value is the same as in Fig. 2). Note that for $r = 0$, one has a perfect specular symmetry of the trajectories $k_n(\alpha)$ about the angle $\alpha = 45^\circ$ since it corresponds to the right triangle billiard and there is a trivial equivalence of triangles for $\alpha \leftrightarrow \beta = \pi/2 - \alpha$ (Fig. 1). This symmetry is naturally broken if $r \neq 0$. Also, for the case of $r = 0$, if $\alpha = 45^\circ$, the billiard is regular [with the exact solutions given by Eq. (2)], presenting degenerate levels and thus actual crossings of some k_n's. In Fig. 12, the soliton-like structures, composed of a large number of branches (especially when $r = 0$), are once more observed in the spectra. Nevertheless, they start to disappear for $\alpha > 45^\circ$ as r increases.

In Fig. 13, we have the three spectra regions indicated in gray in Fig. 12. The behavior discerned in Figs. 3 and 4 is again seen in Fig. 13. However, some extra features can also be detected. We begin considering the case of $r = 0$ and two soliton-like structures, ab and de. The point c (corresponding to an integrable billiard since $\alpha = 45^\circ$ and $r = 0$) is a sort of end point, at which these two solitons terminate. However, the eigenstate morphologies, similar in a and b and in d and e, are different from those in c [see $|\psi_n|^2$ in Figs. 6(a), 6(b), 6(c$_1$), 6(c$_2$), 6(d), and 6(e)]. Also, given the already mentioned symmetry about $\alpha = 45^\circ$ of the $r = 0$ right triangle billiard, as it should be, the state (a) is a simple 90° rotation of the state (e), likewise for (b) and (d). At c, we have a real crossing with two degenerated states. The solutions c_1 and c_2 have been calculated numerically from the BWM. They are exactly the same than those from Eq. (2), respectively, by setting $l = 9$, $m = 19$ and $l = 1$, $m = 21$ (we have compared the numerical and analytic solutions, and by direct eye inspection, one cannot tell the difference between the plots). Moreover, from the BWM, we have found $k = 66.0740$, whereas the exact value is $k = 66.0482\ldots$, thus a difference of only 0.04% (this exemplifies the good numerical precision of the BWM). With the exception of $\alpha = 60^\circ$ (and equivalently $\alpha = 30^\circ$), classical right triangular billiards of arbitrary $\alpha \neq 45^\circ$ are non-integrable, being either pseudointegrable[99] or weakly chaotic depending if α/π is rational or irrational.[93,100–103] Quantically, this rational/irrational interplay arbitrates between intermediate or semi-Poisson to GOE statistics for the level separation;[82,104–106] see Sec. IV. Hence, although c is the ending point of two soliton-like structures, the states c_1 and c_2 morphologies cannot be those along ab and de.

For $r = 0.1$, the soliton-like line fg—say, corresponding to branches i and $i+1$—follows the previously mentioned trends. Actually, we notice that fg is not a so short soliton since the states (not shown) in the branch $i - 1$, just before branch i of f, are very alike the ψ_n's in (f) and (g) of Fig. 13. Also instructive is to

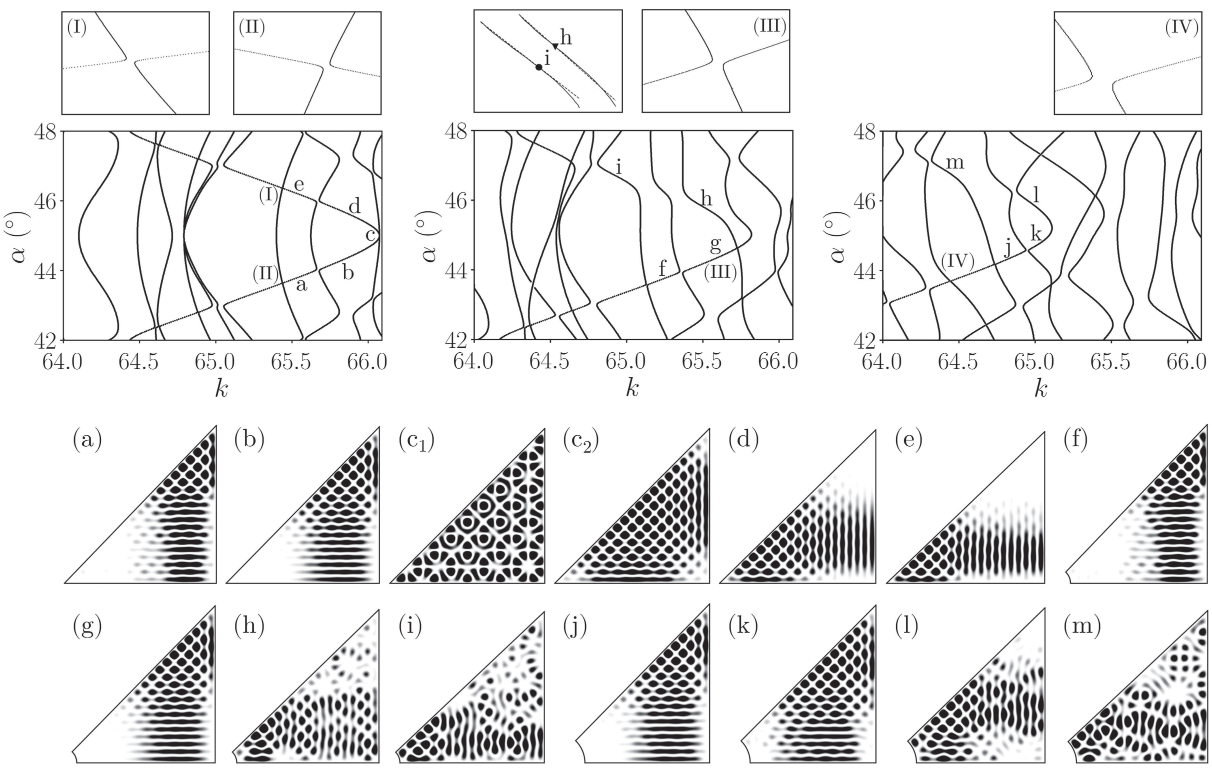

FIG. 13. The same than in Fig. 3, but for the gray regions of Figs. 12(a)–12(c), respectively corresponding to the left ($r = 0.0$), center ($r = 0.1$) and right ($r = 0.2$), panels. The blowups evidence the avoided crossings. Also, the branches of the states i and h ($r = 0.1$) are displayed side by side for comparison, see main text. The dashed lines are the tangents through the points corresponding to h (slop -2.76) and i (slop -2.40). The parameters values are: (a) $k = 65.5931$, $\alpha = 43.9^\circ$; (b) $k = 65.8763$, $\alpha = 44.4^\circ$; (c) $k = 66.0740$, $\alpha = 45^\circ$; (d) $k = 65.9246$, $\alpha = 45.5^\circ$; (e) $k = 65.5340$, $\alpha = 46.2^\circ$; (f) $k = 65.2702$, $\alpha = 43.8^\circ$; (g) $k = 65.6166$, $\alpha = 44.4^\circ$; (h) $k = 65.4992$, $\alpha = 45.8^\circ$; (i) $k = 64.9623$, $\alpha = 46.6^\circ$; (j) $k = 64.8522$, $\alpha = 44.4^\circ$; (k) $k = 65.0315$, $\alpha = 44.8^\circ$; (l) $k = 65.0060$, $\alpha = 45.8^\circ$; (m) $k = 64.4268$, $\alpha = 46.8^\circ$.

contrast the eigenstates (h) (for $\alpha = 45.8^\circ$) and (i) (for $\alpha = 45.6^\circ$) in Fig. 13. They present a somewhat close morphology, even though the two ACs separating the associated branches are very wide compared with those of other soliton-like structures. Indeed, observe the blowups of some much more sharper and narrower ACs in Fig. 13. The key point is that the branches of i and h are segments with similar inclinations (see the details in Fig. 13). Thus, they might be viewed as interpolating a single smooth curve, a requirement for the emergence of soliton-like structures in the $k \times \alpha$ space of our billiard systems.

Finally, for $r = 0.2$, the eigenstates (j) and (k), although much more akin to each other than, e.g., states (l) and (m), do not exhibit a perfect matching: (k) is broader in the horizontal direction. Note that k is in the beginning of the strong bending of its associated branch, making the trajectory k–l to completely change the direction in the $k \times \alpha$ space. This illustrates that an abrupt curvature in a branch tends to terminate a soliton.

APPENDIX C: ANALYSIS OF THE STRAIGHT LINE PORTION OF A SOLITON-LIKE STRUCTURE GENERATED BY VARYING *r*

In Figs. 6–8, we have highlighted the more rounded stretches of some solitons of Fig. 5. Along them, the associated eigenstates display akin morphologies. However, also important is to verify if in

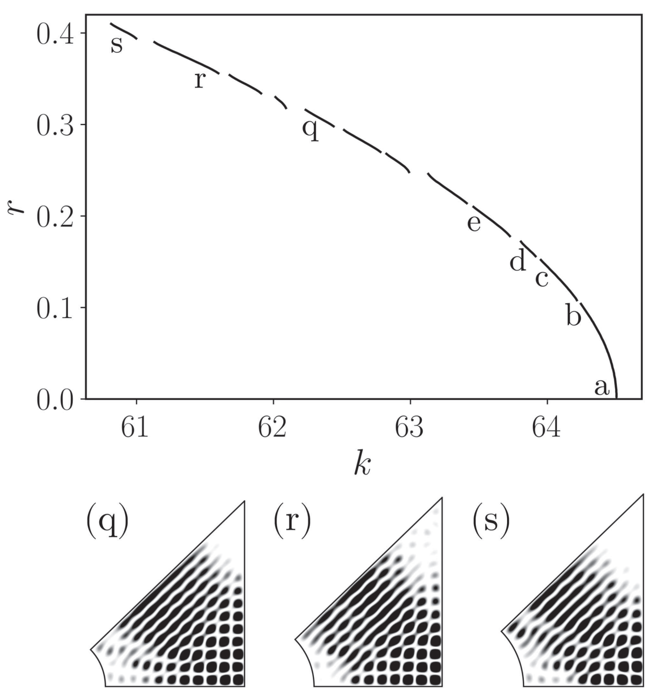

FIG. 14. Details of the soliton-like structure abcde... of Fig. 8 and three extra eigenstates located at branches where the soliton tends to resemble a straight line. The parameter values are (q) $k = 62.5559$, $r = 0.29$; (r) $k = 61.4129$, $r = 0.37$; and (s) $k = 60.3720$, $r = 0.434$.

the straight line portions of such solitons the ψ_n's patterns are still similar. In Fig. 14, we have plotted the full extension of the soliton abcde of Fig. 8 [refer, in Fig. 5(c), to the continuation of the abcde soliton outside the gray region]. We note that the state morphology general trends remain the same [compare (q), (r), and (s) in Fig. 14 with (a)–(e) in Fig. 8]. Particularly, observe (1) the same $|\psi_n|^2$'s structures of maxima and minima parallel to the billiard hypotenuse and toward the right angle corner and (2) the systematic steadily growth, as r increases, of the region around the α angle corner for which the amplitude probability is very small. Actually, we have surveyed many other analogous cases, always finding a good similarity of the states along the entire solitons.

DATA AVAILABILITY

The data that support the findings of this study are available within the article.

REFERENCES

[1] H. G. Schuster and W. Just, *Deterministic Chaos*, 4th ed. (Wiley-VCH, Weinheim, 2005).
[2] M. C. Gutzwiller, *Chaos in Classical and Quantum Mechanics* (Springer, New York, 1990).
[3] R. J. Brown, *A Modern Introduction to Dynamical Systems* (Oxford University Press, Oxford, 2018).
[4] C.-A. Pillet, "Quantum dynamical systems," in *Open Quantum Systems I*, edited by S. Attal, A. Joyce, and C.-A. Pillet (Springer, Berlin, 2006), pp. 107–182.
[5] A. M. O. de Almeida, *Hamiltonian Systems: Chaos and Quantization* (Cambridge University Press, Cambridge, 1992).
[6] G. M. Zaslavsky, *The Physics of Chaos in Hamiltonian Systems*, 2nd ed. (Imperial College Press, London, 2007).
[7] *Handbook of Applications of Chaos Theory*, edited by C. H. Skiadas and C. Skiadas (CRC Press, Boca Raton, FL, 2016).
[8] E. Gutkin, "Billiards in polygons: Survey of recent results," J. Stat. Phys. **83**, 7 (1996).
[9] P. Collas, D. Klein, and H.-P. Schwebler, "Convergence of Hamiltonian systems to billiards," Chaos **8**, 466 (1998).
[10] S. Tabachnikov, *Geometry and Billiards* (AMS, Providence, RI, 2005).
[11] N. Chernov and R. Markarian, *Chaotic Billiards* (AMS, Providence, RI, 2006).
[12] E. Gutkin, "Billard dynamics: An updated survey with the emphasis on open problems," Chaos **22**, 026116 (2012).
[13] U. A. Rozikov, *Mathematical Billiards* (World Scientific, Singapore, 2018).
[14] M. Cencini, F. Cecconi, and A. Vulpiani, *Chaos: From Simple Models to Complex Systems* (World Scientific, Singapore, 2010).
[15] E. P. S. Xavier, M. C. Santos, L. G. G. V. Dias da Silva, M. G. E. da Luz, and M. W. Beims, "Quantum chaos for two interacting particles confined to a circular billiard," Physica A **342**, 377 (2004).
[16] A. Barnett, D. Cohen, and E. J. Heller, "Deformation and dilations of chaotic billards, dissipation rate, and quasi-orthogonality of the boundary wavefunctions," Phys. Rev. Lett. **85**, 1412 (2000).
[17] A. Gusso, M. G. E. da Luz, and L. G. C. Rego, "Anomalous quantum chaotic behaviour in suspended electromechanical nanostructures," J. Phys. A **38**, L639 (2005).
[18] A. Gusso, M. G. E. da Luz, and L. G. C. Rego, "Quantum chaos in nanoelectromechanical structures," Phys. Rev. B **73**, 035426 (2006).
[19] Ya. G. Sinai, *Introduction to Ergodic Theory* (Princeton University Press, Princeton, NJ, 1976).
[20] Ya. G. Sinai, "Dynamical systems with elastic reflections," Russ. Math. Surv. **25**, 137 (1970).
[21] L. A. Bunimovich, "On ergodic properties of certain billiards," Funct. Anal. Appl. **8**, 254 (1974).
[22] L. A. Bunimovich, "Mechanisms of chaos in billiards: Dispersing, defocusing and nothing else," Nonlinearity **31**, R78 (2018).

[23] M. Berry, "Quantum chaology, not quantum chaos," Phys. Scr. **40**, 335 (1989).
[24] O. Legrand and F. Mortessagne, "Wave chaos for the Helmholtz equation," in *New Directions in Linear Acoustics and Vibration: Quantum Chaos, Random Matrix Theory and Complexity*, edited by M. Wright and R. Weaver (Cambridge University Press, Cambridge, 2010), pp. 24–41.
[25] F. Haake, S. Gnutzmann, and M. Kuś, *Quantum Signatures of Chaos*, 4th ed. (Springer, Cham, 2018).
[26] H.-J. Stöckmann, *Quantum Chaos* (Cambridge University Press, Cambridge, 2007).
[27] T. S. Angell and A. Kirsch, "Boundary value problems for the two-dimensional Helmholtz equation," in *Optimization Methods in Electromagnetic Radiation* (Springer, New York, 2004), Chap. 5.
[28] A. Bäcker, "Numerical aspects of eigenvalues and eigenfunction computations for chaotic quantum systems," in *The Mathematical Aspects of Quantum Maps*, edited by M. D. Esposti and S. Graffi (Springer, Berlin, 2003), pp. 91–144.
[29] G. Casati and T. Prosen, "The quantum mechanics of chaotic billiards," Physica D **131**, 293 (1999).
[30] S. M. Abuelenin, "On the spectral unfolding of chaotic and mixed systems," Physica A **492**, 564 (2018).
[31] M. V. Berry and M. Tabor, "Level clustering in the regular spectrum," Proc. R. Soc. A **356**, 375 (1977).
[32] J. Marklof, "The Berry-Tabor conjecture," in *Proceedings of the 3rd European Congress of Mathematics, Barcelona 2000*, edited by C. Casacuberta, R. M. M. Roig, J. Verdera, and S. X. Descamps (Birkhäuser, Basel, 2001), pp. 421–427.
[33] O. Bohigas, M. J. Giannoni, and C. Schmit, "Characterization of chaotic quantum spectra and universality of level fluctuation laws," Phys. Rev. Lett. **52**, 1 (1984).
[34] M. L. Mehta, *Random Matrices*, 3rd ed. (Academic Press, Amsterdam, 2004).
[35] S. Heusler, S. Müller, A. Altland, P. Braun, and F. Haake, "Periodic-orbit theory of level correlations," Phys. Rev. Lett. **98**, 044103 (2007).
[36] S. Nonnenmacher, "Anatomy of quantum chaotic eigenstates," in *Chaos*, edited by B. Duplantier, S. Nonnenmacher, and V. Rivasseau (Birkhäuser, Basel, 2013), pp. 193–238.
[37] M. V. Berry, "Regular and irregular semiclassical wavefunctions," J. Phys. A **12**, 2083 (1977).
[38] P. O.'Connor, J. Gehlen, and E. J. Heller, "Properties of random superpositions of plane waves," Phys. Rev. Lett. **58**, 1296 (1987).
[39] G. Blum, S. Gnutzmann, and U. Smilansky, "Nodal domains statistics: A criterion for quantum chaos," Phys. Rev. Lett. **88**, 114101 (2002).
[40] E. Bogomolny and C. Schmit, "Percolation model for nodal domains of chaotic wave functions," Phys. Rev. Lett. **88**, 114102 (2002).
[41] E. J. Heller, "Bound-state eigenfunctions of classically chaotic Hamiltonian systems: Scars of periodic orbits," Phys. Rev. Lett. **53**, 1515 (1984).
[42] E. B. Bogomolny, "Smoothed wave functions of chaotic quantum systems," Physica D **31**, 169 (1988).
[43] S. Sridhar, "Experimental observation of scarred eigenfunctions of chaotic microwave cavities," Phys. Rev. Lett. **67**, 785 (1991).
[44] F. P. Simonotti, E. Vergini, and M. Saraceno, "Quantitative study of scars in the boundary section of the stadium billiard," Phys. Rev. E **56**, 3859 (1997).
[45] E. Bogomolny and C. Schmit, "Structure of wave functions of pseudointegrable billiards," Phys. Rev. Lett. **92**, 244102 (2004).
[46] A. H. Barnett and T. Betcke, "Quantum mushroom billiards," Chaos **17**, 043125 (2007).
[47] E. Bogomolny, "Formation of superscar waves in plane polygonal billiards," J. Phys. Commun. **5**, 055010 (2021).
[48] L. Kaplan, "Scars in quantum chaotic wavefunctions," Nonlinearity **12**, R1 (1999).
[49] P. J. J. Luukko, B. Drury, A. Klales, L. Kaplan, E. J. Heller, and E. Räsänen, "Strong quantum scarring by local impurities," Sci. Rep. **6**, 37656 (2016).
[50] C. J. Turner, A. A. Michailidis, D. A. Abanin, M. Serbyn, and Z. Papic, "Weak ergodicity breaking from quantum many-body scars," Nat. Phys. **14**, 745 (2018).
[51] W. D. Heiss and A. A. Kotzé, "Quantum chaos and properties of eigenstates," Z. Phys. A **337**, 239 (1990).
[52] D. C. Meredith, "Statistics and scarring of eigenvectors of a shell model," Phys. Rev. E **47**, 2405 (1993).
[53] E. Cuevas, E. Louis, and J. A. Vergés, "Model of quantum chaotic billiards: Spectral statistics and wave functions in two dimensions," Phys. Rev. Lett. **77**, 1970 (1996).
[54] E. J. T. Herrera and L. F. Santos, "Dynamical manifestations of quantum chaos: Correlation hole and bulge," Philos. Trans. R. Soc. A **375**, 20160434 (2017).
[55] S. Tomsovic, A. Lakshminarayan, S. C. L. Srivastava, and A. Bäcker, "Eigenstate entanglement between quantum chaotic subsystems: Universal transitions and power laws in the entanglement spectrum," Phys. Rev. E **98**, 032209 (2018).
[56] A. I. Shnirelman, "On the asymptotic properties of eigenfunctions in the regions of chaotic motion (addendum)," in *KAM Theory and Semiclassical Approximations to Eigenfunctions*, edited by V. F. Lazutkin (Springer-Verlag, Berlin, 1991).
[57] V. I. Klyatskin, "Eigenvalue and eigenfunction statistics," in *Stochastic Equations: Theory and Applications in Acoustics, Hydrodynamics, Magnetohydrodynamics, and Radiophysics* (Springer, Cham, 2015), Vol. 2, pp. 253–260.
[58] D. S. Grebenkov and B.-T. Nguyen, "Geometrical structure of Laplacian eigenfunctions," SIAM Rev. **55**, 601 (2013).
[59] W.-M. Zhang, D. H. Fend, J.-M. Yuan, and S.-J. Wang, "Integrability and nonintegrability of quantum systems: Quantum integrability and dynamical symmetry," Phys. Rev. A **40**, 438 (1989).
[60] A. Chan, A. De Luca, and J. T. Chalker, "Eigenstate correlations, thermalization, and the butterfly effect," Phys. Rev. Lett. **122**, 220601 (2019).
[61] I. C. Percival, "Regular and irregular spectra," J. Phys. B **6**, L229 (1973).
[62] P. Pechukas, "Distribution of energy eigenvalues in the irregular spectrum," Phys. Rev. Lett. **51**, 943 (1983).
[63] T. Yukawa, "New approach to the statistical properties of energy levels," Phys. Rev. Lett. **54**, 1883 (1985).
[64] S.-J. Wang and S. Y. Chu, "Level dynamics: An approach to the study of avoided level crossings and transition chaos," Phys. Rev. A **47**, 3546 (1993).
[65] T. Takami and H. Hasegawa, "Curvature distribution of chaotic quantum systems: Universality and nonuniversality," Phys. Rev. Lett. **68**, 419 (1992).
[66] F. Simmel and M. Eckert, "Avoided crossings: Curvature distribution and behavior of eigenfunctions of pseudointegrable and chaotic billiards," Phys. Rev. E **51**, 5435 (1995).
[67] P. Gaspard, S. A. Rice, H. J. Mikeska, and K. Nakamura, "Parametric motion of energy levels: Curvature distribution," Phys. Rev. A **42**, 4015 (1990).
[68] P. Gaspard, S. A. Rice, and K. Nakamura, "Solitonlike structure in the parametric distortions of bounded-system energy spectra," Phys. Rev. Lett. **63**, 930 (1989).
[69] J. Zakrzewski and D. Delande, "Parametric motion of energy levels in quantum chaotic systems. I. Curvature distributions," Phys. Rev. E **47**, 1650 (1993).
[70] E. Vergini and D. A. Wisniacki, "Localized structures embedded in the eigenfunctions of chaotic Hamiltonian systems," Phys. Rev. E **58**, R5225 (1998).
[71] M. Wilkinson, "Narrowly avoided crossings," J. Phys. A **20**, 635 (1987).
[72] S. W. McDonald and A. N. Kaufmann, "Wave chaos in the stadium, statistical properties of short-wave solutions of the Helmholtz equation," Phys. Rev. A **37**, 3067 (1988).
[73] P. W. O'Connor and E. J. Heller, "Quantum localization for a strongly classically chaotic system," Phys. Rev. Lett. **61**, 2288 (1988).
[74] G. Tanner, "How chaotic is the stadium billiard? A semiclassical analysis," J. Phys. A **30**, 2863 (1997).
[75] A. Bäcker, R. Schubert, and P. Stifter, "On the number of bouncing ball models in billiards," J. Phys. A **30**, 6783 (1997).
[76] M. G. E. da Luz, A. S. Lupu-Sax, and E. J. Heller, "Quantum scattering from arbitrary boundaries," Phys. Rev. E **56**, 2496 (1997).
[77] F. M. Zanetti, E. Vicentini, and M. G. E. da Luz, "Eigenstates and scattering solutions for billiard problems: A boundary wall approach," Ann. Phys. (N. Y.) **323**, 1644 (2008).
[78] F. M. Zanetti and M. G. E. da Luz, "Determining and characterizing families of electronic resonance states in open and closed coupled cavities," Eur. Phys. J. B **85**, 202 (2012).
[79] M. V. Berry, "Quantizing a classically ergodic system: Sinai's billiard and the KKR method," Ann. Phys. **131**, 163 (1981).
[80] A. Bäcker, R. Ketzmerick, S. Löck, and H. Schanz, "Partial Weyl law for billiards," EPL **94**, 30004 (2011).

[81] For our analysis in this work, eventual variations in $\rho(k)$ due to changes in the billiard corners can be neglected.
[82] H. Ch. Schachner and G. M. Obermair, "Quantum billiards in the shape of right triangles," Z. Phys. B **95**, 113 (1994).
[83] H. V. McIntosh, "Symmetry and degeneracy," http://delta.cs.cinvestav.mx/~mcintosh/cellularautomata/OTHER_TOPICS_files/symm.pdf (2002).
[84] Z.-Q. Ma, *Group Theory for Physicists* (World Scientific, Singapore, 2019).
[85] M. V. Berry and M. Wilkinson, "Diabolical points in the spectra of triangles," Proc. R. Soc. London A **392**, 15 (1984).
[86] S. Keshavamurthy, "Fingerprints of a classical resonance on the eigenlevel dynamics of the corresponding quantum Hamiltonian," J. Phys. Chem. A **105**, 2668 (2001).
[87] D. D. de Menezes, M. J. E. Silva, and F. M. de Aguiar, "Numerical experiments on quantum chaotic billards," Chaos **17**, 023116 (2007).
[88] A. S. Pilipchuk and A. F. Sadreev, "Acidental bound states in the continuum in an open Sinai billiard," Phys. Lett. A **381**, 720 (2017).
[89] Y. G. Sinai and N. Chernov, "Ergodic properties of certain systems of two-dimensional discs and three-dimensional balls," Russ. Math. Surv. **42**, 181 (1987).
[90] G. Casati, B. V. Chirikov, and I. Guarneri, "Energy-level statistics of integrable quantum systems," Phys. Rev. Lett. **54**, 1350 (1985).
[91] T. A. Brody, "A statistical measure for the repulsion of energy levels," Lett. Nuovo Cimento **7**, 482 (1973).
[92] B. Cipra, R. M. Hanson, and A. Kolan, "Periodic trajectories in right-triangle billiards," Phys. Rev. E **52**, 2066 (1995).
[93] P. W. Hooper, "Periodic billiard paths in right triangles are unstable," Geom. Dedicata **125**, 39 (2007).
[94] N. Chernov and S. Troubetzkoy, "Ergodicity of billiards in polygons with pockets," Nonlinearity **11**, 1095 (1998).
[95] E. B. Bogomolny, "Semiclassical quantization of multidimensional systems," Nonlinearity **5**, 805 (1992).
[96] A. M. O. de Almeida, "Exact Bogomolny sections for separable systems," J. Phys. A **27**, 2891 (1994).
[97] M. R. Haggerty, "Semiclassical quantization using Bogomolny's quantum surface of section," Phys. Rev. E **52**, 389 (1995).
[98] J. S. E. Ortiz and A. M. O. de Almeida, "Bogomolny section for the stadium: I. Quantum theory," J. Phys. A **30**, 7301 (1997).
[99] P. J. Richens and M. V. Berry, "Pseudointegrable systems in classical and quantum mechanics," Physica D **2**, 495 (1981).
[100] R. Artuso, G. Casati, and I. Guarneri, "Numerical study on ergodic properties of triangular billiards," Phys. Rev. E **55**, 6384 (1997).
[101] S. Troubetzkoy, "Periodic billiard orbits in right triangles," Ann. Inst. Fourier **55**, 29 (2005).
[102] R. E. Schwartz, "Billiards obtuse and irrational," https://www.math.brown.edu/reschwar/Papers/intel.pdf (unpublished).
[103] F. Valdez, "Infinite genus surfaces and irrational polygonal billiards," Geom. Dedicata **143**, 143 (2009).
[104] B. Grémaud and S. R. Jain, "Spacing distributions for rhombus billiards," J. Phys. A **31**, L637 (1998).
[105] E. B. Bogomolny, U. Gerland, and C. Schmit, "Models of intermediate spectral statistics," Phys. Rev. E **59**, R1315 (1999).
[106] T. Gorin, "Generic spectral properties of right triangle billiards," J. Phys. A **34**, 8281 (2001).